ELSEVIER

Chemical Geology 239 (2007) 228–249

CHEMICAL GEOLOGY
INCLUDING
ISOTOPE GEOSCIENCE

www.elsevier.com/locate/chemgeo

Experimental constraints on element mobility from subducted sediments using high-P synthetic fluid/melt inclusions

Carl Spandler [a,*], John Mavrogenes [a,b], Jörg Hermann [a]

[a] *Research School of Earth Sciences, Australian National University, Canberra, 0200, Australia*
[b] *Department of Earth and Marine Sciences, Australian National University, Canberra, 0200, Australia*

Accepted 14 October 2006

Editor: S.L. Goldstein

Abstract

A series of hydrothermal piston-cylinder experiments have been performed to determine the composition of representative fluids and fluid/melt/rock interaction in subduction zones. Experiments were conducted under H_2O saturated conditions at 2.2 GPa over a temperature range from 600–750 °C. The experiments contained synthetic, trace-element-doped pelitic starting material and fractured quartz chips to trap and preserve synthetic fluid/melt inclusions. Pelite residues from the subsolidus experiments (600–650 °C) consist of an eclogite-facies mineral assemblage including quartz, phengite, epidote, rutile, garnet, amphibole, apatite, and zircon. Coexisting hydrous fluids are expected to be completely buffered for trace elements by this mineral assemblage. At 2.2 GPa the wet solidus for the pelitic starting material is located at approximately 675 °C and hydrous fluid and melt coexist as immiscible phases at least up to 750 °C. Residue phases in the supersolidus experiments (700–750 °C) are garnet, rutile, and zircon, which suggest that HREE and HFSE are largely retained in slab residues during very high degrees of H_2O saturated melting.

Laser ablation ICPMS analysis and quantification of trapped fluid inclusions from the experiments indicate that subsolidus hydrous fluids released from subducted sediments have relatively high LILE contents compared to REE and HFSE, but overall are remarkably dilute. Total solute contents are approximately 5 wt.%, of which >75% is SiO_2 and around 15% is $Na_2O + Al_2O_3$. The experimental results are used to show that subducting sedimentary rocks do not undergo significant element loss during metamorphic dehydration up to eclogite facies. If these fluids are representative of aqueous fluids released at sub-arc depths then simple slab dehydration models may be unable to account for element transfer from the slab to arc magmas. Instead, element recycling through subduction zones may be a product of complex fluid-melt-rock interaction processes involving multiple slab components.

Keywords: Subduction; Fluid; Melt; Fluid inclusions; Trace elements; LA-ICP-MS

1. Introduction

Volatile and element recycling through subduction zones is fundamental to arc magma-genesis, continental crust formation and the geochemical evolution of the mantle. It is often assumed that hydrous fluids derived from dehydration of the sinking slab not only cause melting of the mantle wedge, but also transport 'fluid mobile' elements from the slab to the mantle wedge (e.g., Tatsumi, 2005). By contrast, geochemical and isotopic criteria are commonly cited as evidence that arc magmas contain multiple slab components including fluid and

* Corresponding author. Now at Institute of Geological Sciences, University of Bern, Switzerland. Tel.: +41 31 631 8768.
E-mail address: Spandler@geo.unibe.ch (C. Spandler).

0009-2541/$ - see front matter © 2006 Elsevier B.V. All rights reserved.
doi:10.1016/j.chemgeo.2006.10.005

melt derived from subducted oceanic crust and metasedimentary rocks (Hawkesworth et al., 1993; Class et al., 2000; Elliott, 2003). In sum, the processes leading to mass transfer from the subducting slab and the nature of the transferring agents remain poorly constrained. A detailed understanding of these processes is crucial for developing accurate geochemical and geophysical models of subduction zones and arc magmatism.

Experimental investigations of subduction-zone processes have focussed on determining the mineral stabilities and phase relations of the major rock-types of subducting crust (Liu et al., 1996; Ono, 1998; Ulmer and Trommsdorff, 1999; Poli and Schmidt, 2002; Hermann, 2002; Forneris and Holloway, 2003). This information is vital for predicting release of hydrous fluid from the slab during subduction, but as yet there have been very few attempts to experimentally constrain the nature and composition of these fluids. This is primarily due to the technical difficulty of conducting meaningful hydrothermal experiments at conditions relevant to subduction (Kessel et al., 2004; Hack and Mavrogenes, 2006). Critical constraints include conducting experiments at appropriate pressure (P) and temperature (T) conditions and ensuring fluids are buffered during experiments by a residue with an appropriate high-P mineral assemblage. In order to accurately determine fluid compositions experiments also need to be designed to account for modification of the fluid during quenching and allow complete separation of fluid and residue after experiment completion.

Aqueous fluid is regarded as the dominant fluid type evolved from subducting slabs (Scambelluri and Philippot, 2001) and subducted sedimentary rocks are regarded as the principal source of many key elements that are enriched in arc magmas (Plank and Langmuir, 1993; Elliott, 2003). Therefore, determining accurate sediment-derived fluid and melt compositions at high P are critical for understanding mass transfer from the slab to mantle wedge. We have conducted a series of high-P hydrothermal piston-cylinder experiments designed to investigate the interaction and composition of aqueous fluid, melt, and pelitic sediment during subduction. The experiments use large cold-sealed silver capsules, which allow precise measurement of fluid-rock ratios and recovery of large volumes of run products for geochemical and mineralogical analysis. Furthermore, care has been taken to ensure that appropriate trace-element-buffering mineral phases were formed in the solid residue during subsolidus runs. Fluid compositions and fluid-melt phase relations were determined by analysis of fluid inclusions trapped in quartz during the experiments. Synthetic fluid inclusions trapped during experiments under equilibrium conditions represent preserved and complete samples of fluids produced at run conditions. Therefore analysis of these inclusions provides unsurpassed information on the nature and composition of fluids at elevated P and T. This study is the first to use synthetic fluid inclusions to quantify representative subduction-zone fluids.

The experimental results are used to evaluate phase relations in subducting sedimentary rocks and constrain the composition of fluids equilibrated with pelitic rocks under eclogite-facies conditions. These data also place constraints on the geochemical evolution of subducting slabs, which has direct consequences for the generation of arc magmatism, global element recycling and the evolution of the mantle and crust.

2. Experimental strategy

To avoid problems associated with recovering and preserving high-P experimental fluids, we employ techniques of trapping and preserving synthetic fluid inclusions in quartz during piston cylinder experiments. The trapping and subsequent analysis of synthetic fluid inclusions in quartz is routinely used to quantify hydrothermal fluid compositions and element solubilities at relatively low P (e.g., Sterner and Bodnar, 1984; Loucks and Mavrogenes, 1999; Simon et al., 2005), but as yet have not been used for high-P experiments. Therefore, we have conducted two preliminary experiments containing fractured quartz and water to test the suitability of the fluid inclusion technique for modelling subduction-zone conditions. Subsequent experiments also contained a pelitic starting material to model fluid-melt-rock interactions under eclogite-facies conditions. Quartz-hosted fluid inclusions recovered from these experiments are interpreted to represent quenched samples of fluid equilibrated at run conditions. Therefore bulk analysis of these inclusions allows for direct quantification of high-P fluids. A significant advantage of this technique is that analytical problems associated with modification of the fluid on quenching are largely avoided.

2.1. Starting material synthesis

Continental-derived materials provide the bulk of the trace-element budget of subducting sedimentary piles and hence are most likely to influence the composition of arc magmas (Rea and Ruff, 1996; Plank and Langmuir, 1998). Therefore, for this study a starting material has been synthesized that has a major-element composition similar to average global subducting sediment (GLOSS; Table 1; Plank and Langmuir, 1998) and the average

Table 1
Composition of the experimental pelite starting material (EPSM), and global average subducting sediment (GLOSS)

	EPSM	GLOSS (P and L)
SiO_2	68.35	65.31
TiO_2	0.66	0.69
Al_2O_3	14.91	13.28
FeO	4.63	5.81
MnO	0.11	0.36
MgO	3.03	2.77
CaO	2.41	6.63
Na_2O	2.57	2.71
K_2O	2.88	2.27
Total	99.55	99.83
P	1413	829
Sc	56	14.6
Ti	3626	4137
Mn	802	2788
Rb	225	63.8
Sr	215	364
Y	60	33.2
Zr	202	145
Nb	57	9.97
Cs	241	3.88
Ba	1174	865
La	163	32.1
Ce	68	63.9
Nd	60	30.1
Sm	66	6.45
Eu	61	1.46
Gd	58	5.87
Dy	55	5.56
Er	57	3.26
Yb	60	3.08
Hf	48	4.53
Ta	57	0.70
Pb	213	22.2
Th	238	7.71
U	532	1.87

Note: GLOSS calculated volatile-free from Plank and Langmuir (1998).

upper continental crust (Taylor and McLennan, 1985). The starting material was produced with high levels (50–1500 ppm) of key trace elements using a 'sol–gel' method (Luth and Ingamells, 1965) in order to eliminate problems of sluggish reaction of refractory minerals during experiments and limitations of analysing low trace-element concentrations in run products. Most major elements and all trace elements were combined as nitrate solutions and mixed with tetraethyl orthosilicate ($Si(C_2H_5O)_4$) and slowly dried to a gel. The gel was then heated to 1000 °C for 12 hours to drive off the nitrates. The residual powder was then combined with appropriate amounts of Al_2O_3, TiO_2 and MnO powders, finely milled and then fused at 1500 °C and quenched to glass. Multiple analyses of the glass for major elements (by EDS) and trace elements (by LA-ICPMS) indicate homogeneity within analytical precision. Iron was then added to the glass in the form of synthetic fayalite. The fayalite and glass mix was ground for 30 min to form a fine powder. In order to promote garnet growth in the experiments, 10–50 μm pyrope seeds from the Dora Maira whiteschists (Hermann, 2003) were added as 2% of the starting mix. The final starting material composition, herein labelled experimental pelite starting material (EPSM), is presented in Table 1.

2.2. Experimental setup

All experimental runs were conducted in a 15.9 mm end-loaded piston cylinder apparatus at the Research School of Earth Science (RSES), Australian National University (ANU). The capsules and experimental assemblies were specifically designed to investigate hydrothermal conditions under relatively high-P, low-T conditions. Large silver capsules (Fig. 1) were used in order to maximize the capsule volume and avoid problems of H loss and Fe alloying. These capsules have an inner volume of around 500 mm^3 after sealing, which is an order of magnitude larger than capsules typically used in a standard 12.7 mm piston-cylinder assembly. The capsules were sealed using a precisely-machined silver lid (Fig. 1) that was cold pressed onto the capsule using the technique described by Hack and Mavrogenes (2006). A specially-designed swaging tool was used to seal the lid onto the capsule by folding the thin upper walls of the capsule over the outer rim of the lid (Fig. 1). To accommodate the large capsule, an assembly of a talc outer sleeve, graphite heater and thin (0.5 mm) talc inner sleeve was used with pyrophyllite spacers above and below the capsule. Temperature was controlled using a type-B thermocouple ($Pt_{94}Rh_6$/$Pt_{70}Rh_{30}$) and a Eurotherm temperature controller and is accurate to within 5 °C. Care was taken to locate the capsule within the hotspot of the assembly, although the high thermal conductivity of silver and large volume of silver and water in the experiments serve to minimize T gradients across the assembly. Furthermore, the thermocouple tip was designed to be in direct contact with the silver lid in order to minimize the difference between measured and actual run temperatures. Extensive testing of a similar capsule design by Hack and Mavrogenes (2006) has shown that the T within the capsule and at the thermocouple site differs by less than 10 °C. Nonetheless, examination of run products indicated that slight T gradients (<10 °C) existed within the capsule during experimental runs, as discussed below. Microprobe analysis of a thermocouple tip after an experiment has confirmed that alloying between the thermocouple wire

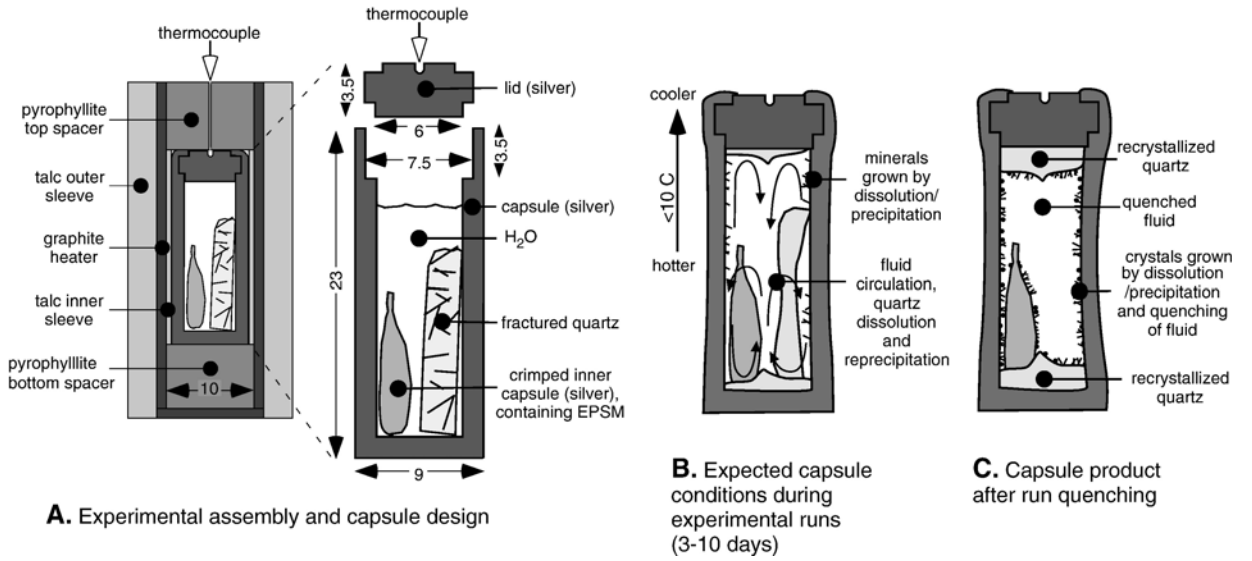

Fig. 1. A. Design and specification of the capsule and assembly used in the piston-cylinder experiments. All measurements are in millimetres. B. Expected conditions within the capsule during experimental runs. Note, the slight temperature gradient through the capsule promotes fluid circulation leading to dissolution and reprecipitation of quartz, and precipitation of crystals (phengite, Na-mica, rutile, apatite) on the capsule walls. C. Capsule after experiment quenching. Note, crystals precipitated during the experiment and during quenching of the experiment are found on the capsule walls. The quartz has completely re-precipitated at the ends of the capsule and now contains primary fluid/melt inclusions.

and the silver was insignificant, and therefore does not compromise the accuracy of the thermocouple. The difference between the measured and capsule T is assumed to be 10 °C for all experiments.

Pressure corrections of −10% are commonly assumed in talc-assembly piston-cylinder experiments of short duration (e.g., Green et al., 1966). However, Bose and Ganguly (1995) demonstrated that nominal P approaches the actual sample P over time as the cell compacts and friction is eliminated. In all of our experiments the nominal P continually dropped for the first 3 to 4 days by a total of around 10%. The P was continually adjusted back to starting nominal P and remained steady after 4 days. As talc is not expected to dehydrate under the P–T conditions of these experiments and all experiments are in excess of 4 days in duration, it is expected that all assembly friction was eliminated during the runs. Therefore, no friction correction is applied to the P measurements. Oxygen fugacity was not buffered in the experiments. However, some preliminary experiments were loaded with H_2O and either Ni or NiO. In either case a mixture of Ni and NiO was recovered from these runs, which indicates that oxygen fugacity conditions were close to the Ni–NiO buffer during the experiments (log fO_2 of −18 at 650 °C).

All experiments were loaded with 200–330 ml of Milli-Q® purified water and 240–520 mg of clear inclusion-free quartz. In order to promote fluid-inclusion entrapment in healing fractures during the runs, the quartz was pre-fractured by heating to 350 °C and quenching in water. To prevent deformation and rupturing of the capsule during ramping and quenching of the experimental runs, P and T were increased or decreased synchronously along the relevant pure-water isochore at a rate of 50 °C per min. This procedure also minimizes decrepitation of fluid inclusions on quenching.

2.3. Details of experimental runs

Two initial experimental runs containing only water and quartz were conducted to test trapping and preservation of fluid inclusions at run conditions and during quenching, and to test the P and T calibrations of the cell (Table 2). The masses of the loaded capsules before and after the runs were very similar, indicating that the capsules had not leaked during the runs. All other experiments (PFI 2-7) contained approximately 60 mg of the EPSM together with the pre-fractured quartz and water (Fig. 1). The EPSM was compressed into a second inner silver capsule, which was only loosely crimped closed. Confining the starting powder in the unsealed inner capsule promotes metamorphic mineral growth at run conditions without limiting the interaction between the fluid and EPSM. Furthermore, separation of the EPSM from the bulk of the fluid avoids significant

Table 2
Details of experimental runs

Run no.	Pressure (GPa)	Temperature (°C)	Duration (hours)	Fluid/EPSM ratio	Major phases	Accessory phases
Test 1	1.0	650	149	–	f	
Test 2	1.5	650	119	–	f	
PFI 3	2.2	600	452	4.48	*ep*, *phg*, *cld*, *Na–Mgsil**, *tlc*, (f)	zrc, ap, gt, rt
PFI 2	2.2	650	340	3.72	*gt*, *ep*, *phg*, *amp*, *cld*, (f)	zrc, ap, rt
PFI 7	2.2	675	310	>1.7	*gt*, *rt*, *phg*, (m, f)	zrc, ep, ky*, chd
PFI 4	2.2	700	260	4.55	*gt*, *rt*, (m, f)	zrc,
PFI 6	2.2	750	120	4.06	gt, rt, (m, f)	zrc, mz

Notes: Quartz was present in all runs. * = possible metastable phases. Mineral abbreviations, f = fluid, m = melt, gt = garnet, rt = rutile, zrc = zircon, ap = apatite, ep = epidote, cld = chloritoid, phg = phengite, Na–Mgsil = Na–Mg sheet silicate, tlc = talc, amp = amphibole, ky = kyanite, mz = monazite. Phases in italics were identified by both SEM and XRD.

contamination of the pelitic residue by phases formed from the fluid on quenching of the experiment and allows the EPSM residue to be easily recovered after the experiment.

Five successful experiments were performed as a temperature series from 600 °C to 750 °C at 2.2 GPa (Table 2). In all of these experiments fluid/rock ratios exceeded 3:1 in order to retain an aqueous fluid phase at run conditions. In all experiments except PFI 7 there was no mass loss from the capsules during the runs, indicating that fluid leakage had not occurred. Some fluid was lost from PFI-7 during the run, as the final capsule weight was 100 mg lower than the initial mass. After the experiments, the capsules were pierced by drilling a small hole through the base of the capsule. Once pierced, fluid was extracted from the capsule with a micro-syringe and then weighed. Fluid volumes of between 50 and 200 mg were extracted for all runs (including PFI 7), confirming that all experiments were saturated with hydrous fluid. The capsules were then opened and the EPSM residue and quartz chips removed. Material precipitated on the capsule walls during quenching was also collected for petrographic analysis. A small amount of the EPSM residue was mounted in 25.4 mm diameter epoxy discs for examination and analysis. EPSM residue from the subsolidus run was also used for XRD analysis. 1 mm-thick slices of doubly polished quartz chip were prepared for inclusion analysis.

2.4. Timing of fluid inclusion entrapment

For several experiments thermocouple shearing occurred during the first few days, leading to loss of temperature control. Although these experiments were immediately quenched and are regarded as failed experiments, the capsule contents were examined in detail to help constrain timing of fluid inclusion formation. The quartz chips from these experiments had not experienced significant healing and fluid inclusion entrapment, even after up to 3 days at run conditions. However, SEM and XRD analysis of the residues of these failed experiments indicates that eclogite-facies minerals such as almandine, phengite, rutile, epidote, and amphibole had already grown. By contrast, the original fractured quartz chips loaded into the successful experiments (5–10 days run duration) had completely dissolved and reprecipitated at the top and bottom of the capsules during these experiments (Fig. 1B,C). We interpret this feature to derive from fluid circulation driven by the slight temperature gradient (<10 °C) across the capsule. This fluid circulation caused dissolution of quartz from the central slightly hotter zone of the capsule and precipitation at the cooler top and bottom of the capsule. The quartz recrystallised in this manner contains abundant fluid inclusions. Collectively, these results verify that fluid inclusion entrapment occurred while the fluid composition was buffered by a high P mineral assemblage. The failed and successful experiments were quenched under similar conditions, but well-formed fluid inclusions were only found in quartz chips from the successful experiments. This observation indicates that most of the inclusions in the successful experiments were trapped prior to quenching. Therefore, we are confident that the fluid inclusions preserved in quartz from all successful experiments represent samples of fluid trapped at run conditions and in equilibrium with high-P mineral assemblage.

3. Analytical techniques

3.1. Fluid inclusion heating/freezing and density calculations

Homogenization temperatures of quartz-hosted fluid inclusions were measured using a USGS fluid inclusion heating/freezing stage mounted on a video-equipped optical microscope at the Department of Earth and

Marine Sciences (DEMS), ANU. Individual inclusions were heated multiple times to precisely measure the homogenization temperatures (T_h). Temperature was calibrated against the freezing and critical points of pure water and is accurate to ±1 °C. The density of inclusions was calculated using the measured T_h, the PTV data for pure water from Haar et al. (1984) and the MacFlinCor software program (Brown and Hagemann, 1995). Effects of thermal expansion and contraction of quartz on fluid inclusion densities are expected to be less that 1% at the run conditions (Hack and Mavrogenes, 2006), so these effects are ignored in fluid density calculations.

3.2. Solution chemistry

Solutions extracted from the capsules were diluted into a 2% HNO_3 matrix down to a 100:1 concentration. Prior to analysis and dilution, 1000 ppm of In was added in solution to serve as an internal standard. The solutions were analysed for In, Al, K, Mg, Ca, and Na using a Varian Vista Pro axial inductively-coupled plasma atomic emission spectrometer (ICP-AES) housed at DEMS, ANU. Samples were calibrated against a blank and 10 ppm and 100 ppm multi-element standards. Three replicates were collected per sample. All element concentrations were well above the detection limits of 2–100 ppb.

For trace element (Rb, Sr, Y, In, Cs, Ba, La, U) analyses, samples diluted to 100:1 and 1000:1 concentration were run on a Vista Ultramass quadrupole ICP Mass Spectrometer at DEMS, ANU. Data was calibrated against a blank and 100 ppb multi-element standard. Five replicates were collected per sample, with 25 scans per replicate and 195 ms scan time. All elements measured were above the detection limits of 0.5–2 ppb, except Y and U in PFI 2. Yttrium and U in PFI 2 are below detection limits, so the relevant detection limits are regarded as maximum concentrations.

3.3. Identification of residual minerals

Due to their very fine grainsize (<30 μm) the EPSM residues and quenched mineral precipitates from the capsule walls were examined using a JEOL 6400 scanning electron microscope (SEM) housed at the Electron Microscope Unit, Research School of Biological Sciences, ANU. Quantitative major element analysis of garnet and rutile, and qualitative analysis of all other minerals was conducted using an energy-dispersive spectrometer equipped to the SEM. Accelerating voltage, beam current, and counting time were set at 15 kV, 1 nA and 100 s respectively.

Residue powders from experiments PFI 2, PFI 3 and PFI 7 were also analysed for major (mode > 5%) mineral phases by XRD. The EPSM residue samples were ground in an agate mortar with acetone and applied onto a low background holder (oriented quartz crystal). Powder diffraction data were collected at room T with a Siemens D501 diffractometer at DEMS, ANU. The diffractometer was equipped with a curved graphite monochromator, a scintillation detector, and CuKα radiation was used. Scans were recorded in one pass from 2° to 70° 2-theta, using a step width of 0.02° and a scan speed of 1° per min. Results were interpreted using the Siemens software package Diffrac*plus* Eva 2000, which uses the PDF database.

3.4. Bulk compositions of residues, quenched melt, and capsule materials

Approximately 50% of the EPSM residual powders from subsolidus experiments PFI 2 and PFI 3 were fused with Li tetraborate ($Li_2B_4O_7$) flux (flux-sample ratio = 3:1) at 1100 °C for 30 min and then quenched. The glasses were then mounted in epoxy and polished for analysis. The Li-Borate glasses, together with quenched melt in runs PFI 4, PFI 6, and PFI 7 were analysed for major elements using a defocused beam by EDS using a JEOL 6400 SEM, as described above. Accelerating voltage, beam current, and counting time were again set at 15 kV, 1 nA, and 100 s respectively. At least 5 analyses of each sample were conducted to confirm sample homogeneity.

Trace-element concentrations of the quenched melt and Li-borate glasses were acquired by laser ablation, inductively-coupled plasma mass spectrometry (LA-ICPMS) at the RSES, ANU. Instrument details and operating conditions are given in Table 3. Counting time

Table 3
LA-ICPMS specifications and operating conditions

Instrument specifications		
ArF 193 nm EXCIMER laser interfaced with an Agilent 7500 quadrupole ICPMS via a custom-built sample cell and teflon sample tubing		
Operating conditions	Glass analyses	Fluid inclusion analyses
Laser pulse rate	5 Hz	10 Hz
Laser power	100 mJ	120 mJ
Laser aperture on sample	70 μm	30–70 μm
Carrier gas flow	0.3 l/s He, 0.95 l/s Ar	0.3 l/s He, 0.95 l/s Ar
Max. oxide production	<0.4% $Th0^+/Th^+$	<0.4% $Th0^+/Th^+$

Note: Laser aperture for fluid inclusions adjusted based on inclusion size.

was 20 s for the background and 60 s for sample analysis. Instrument calibration was against NIST 612 glass using the reference values tabulated by Spandler et al. (2003). ^{27}Al was employed as the internal standard isotope, based on Al_2O_3 concentrations previously measured by EDS. At least 4 analyses of each sample were conducted.

Capsule materials were analysed for a range of elements (Fe, Nb, Ta, Zr, Ti, Al, U, Th, Ag, Pb) both before and after experimental runs in order to test for metal alloying with the silver capsule during the runs. Sections of capsule material were analysed by LA-ICPMS using a 32 μm spot size and ^{107}Ag and ^{109}Ag as internal standard isotopes. The concentrations of all elements except Pb were below detection (<0.05 ppm) in capsule materials both before and after experimental runs indicating that there was insignificant alloying of these metals with the capsule during the experiments. By contrast, Pb was found to be enriched by around 25 times immediately adjacent to the inner wall of the capsule and remain elevated compared to starting Pb levels in the capsule at least 200 μm distant from the inner capsule wall. Due to this Pb loss to the capsule, Pb data presented is only used for calculating solid/fluid partition coefficients.

3.5. Fluid/melt inclusion geochemistry

Experimental fluid/melt inclusions trapped in quartz were analysed for 20 elements by LA-ICPMS, as described in Table 3. Analyses were again standardized against NIST 612 glass. The time resolved spectra obtained from ablation of a large fluid inclusion from PFI 2 is given in Fig. 2. Spectra of the clean quartz host on either side of the inclusions were used for host subtraction during data reduction. Inclusion analyses close to the quartz surface (<10 μm) were not used due to potential elemental interferences from surface contamination (Fig. 2). In order to achieve a sufficient analytical signal from the inclusions dwell times for each element (except ^{29}Si) were set to 25 ms. ^{29}Si was counted for 10 ms in each mass sweep. Consequently, the time for one complete mass sweep was approximately 0.5 s. As ablation of most fluid inclusions produced a short (<5 s) transient signal, these long mass sweep and element dwell times may have been insufficient for completely representative sampling of all of the analysed inclusions (Pettke et al., 2000). Therefore, at least 30 fluid inclusions were analysed from each of the subsolidus experiments (PFI 2 and PFI 3) and at least 20 inclusions were analysed from each of the supersolidus experiments (PFI 4 and PFI 6). Analyses of 16 inclusions from PFI 3 and 12 inclusions from PFI 2 produced distinct peaks of elevated element counts that were unaffected by surface contamination in the time-resolved spectra (Fig. 2). These inclusions produced relatively consistent element ratios and were used to calculate the composition of the fluid in equilibrium with the EPSM at the experimental run conditions. Details of the internal standardization are presented in the Results section below. Further details of fluid inclusion analysis and quantification are discussed in Günther et al. (1998), Heinrich et al. (2003) and Allan et al. (2005).

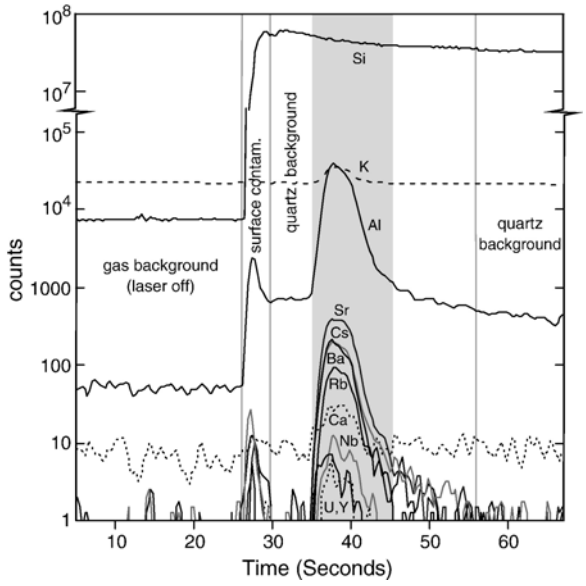

Fig. 2. Time resolved LA-ICPMS spectra of a quartz-hosted fluid inclusion analysis from run PFI 2 (650 °C). For graphical purposes only selected elements are displayed. The first 26 s of the profile represents the gas background without the laser on. The laser is fired at 26 s, causing elevated element counts for 4 s due to contamination on the surface of the quartz crystal. Clean quartz is subsequently ablated until the inclusion is sampled (grey field) from 35 to 45 s, after which clean quartz is again ablated. Host subtraction from the inclusion is conducted by extrapolation between the quartz background sampled before and after the inclusion.

4. Results

4.1. Test experiments

Experimental run TEST 1 was designed to check the P–T calibration of the experimental setup. Nominal run conditions were set to 1.0 GPa and 650 °C in order to trap pure water fluid inclusions with densities of <1.0 g/cm^3. Subsequent T_h measurements of these inclusions were used to calculate the density of the trapped fluids and hence provide an independent constraint on the P–T

conditions of the run. The equation-of-state of water of Brodholt and Wood (1993) was used to relate fluid density to P–T conditions as this equation-of-state is consistent with P–T–V data from synthetic fluid inclusions trapped at ≥1.0 GPa (Brodholt and Wood, 1994; Withers et al., 2000).

The quartz chip recovered from TEST 1 contained numerous (>100) fluid inclusions. Most inclusions range in size from 5 to 30 μm and are clearly isolated from surrounding inclusions. A vapour bubble occupies around 10% of the volume of all inclusions at room T (Fig. 3A). Homogenisation temperatures (T_h) measured for 31 inclusions range from 148.5–160.1 °C, although only three large inclusions had T_h of over 155 °C. These three inclusions are expected to have suffered stretching during quenching of the run and hence were not used for fluid density calculations. The average T_h of the remaining 28 inclusions is 151 °C, which equates to a fluid density of 0.916 g/cm^3. The isochore corresponding to this fluid density intersects a pressure value of 0.99 GPa at 650 °C, which is remarkably consistent with the nominal run conditions (1.0 GPa, 650 °C). This result confirms the accuracy of the P–T calibration of the experimental setup and indicates that most of the fluid inclusions were trapped at run conditions and survived quenching without significant modification.

Experiment TEST 2 was designed to trap and preserve fluid inclusions of density >1.0 g/cm^3. Pure H_2O fluid inclusions trapped under the nominal run conditions of 1.5 GPa and 650 °C should have a density of 1.03 g/cm^3. Quartz chips recovered from the run contained numerous fluid inclusions trapped along healed fractures that range in size from 5–50 μm (Fig. 3B). Vapour bubbles are absent from all inclusions at room T, indicating that the inclusions consist of fluid of densities >1.0 g/cm^3. This result further confirms the accuracy of the P–T calibrations and proves the capability for trapping and preserving primary fluids as inclusions in high-P experiments.

4.2. EPSM-bearing experiments

Five successful experiments containing the EPSM were conducted at 2.2 GPa and temperatures ranging

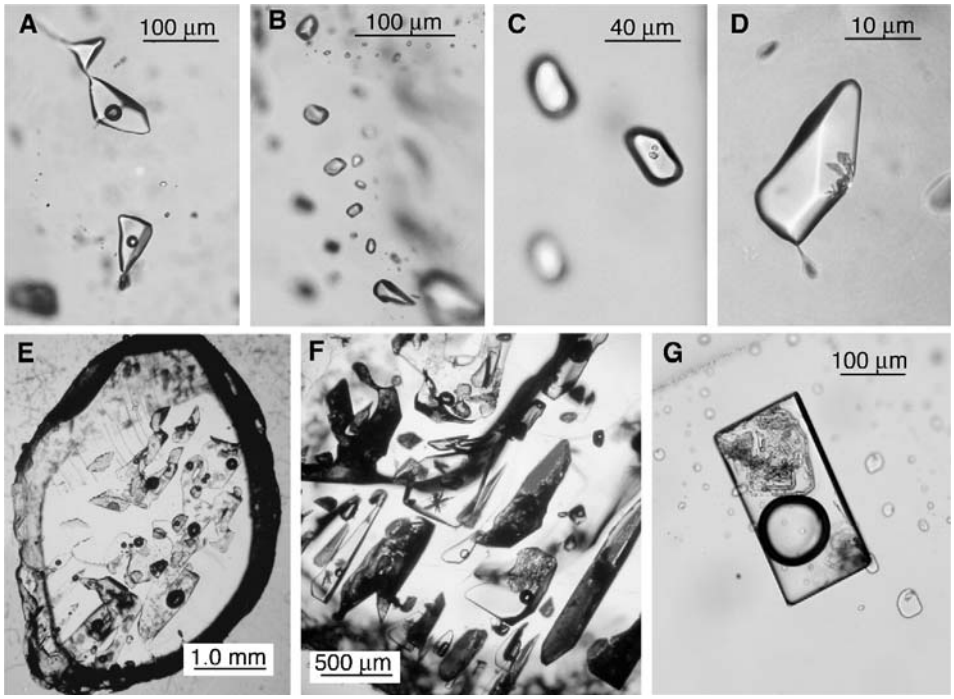

Fig. 3. Photomicrographs of synthetic fluid and melt inclusions trapped in quartz during experiments. A. Pure water inclusions with distinct vapour bubbles from experiment TEST 1 (1.0 GPa, 650 °C). B. high-density (>1.0 g/cm^3) pure water inclusions from experiment TEST 2 (1.5 GPa, 650 °C). C. High-density fluid inclusions from experiment PFI 3 (2.2 GPa, 600 °C). Note, the distinct daughter crystals in the inclusion in focus. D. High-density fluid inclusions from experiment PFI 2 (2.2 GPa, 650 °C). Note, the cluster of daughter crystals. E. Quartz chip from experiment PFI 7 (2.2 GPa, 675 °C) with abundant large fluid/melt inclusions. F. Cluster of large quasi-rectangular fluid/melt inclusions from experiment PFI 4 (2.2 GPa, 700 °C). G. Large rectangular fluid/melt inclusion within a trail of smaller fluid/melt inclusions from PFI 4 (2.2 GPa, 700 °C). Note, the large vapour bubbles and complex daughter crystals in the inclusions.

from 600–750 °C. These experiments allow us to define the phase relations and fluid-saturated solidus of the EPSM, and have provided samples of fluid and melt (as fluid inclusions or as quenched glass) formed at run conditions. Analysis of these fluid and melt samples allows us to constrain the composition of representative subduction-zone fluids and fluid/solid partition coefficients for a range of elements.

4.2.1. Phase relations

4.2.1.1. PFI 3 (600 °C, 2.2 GPa). Due to the fine grainsize (~1–10 μm), residues of the EPSM extracted from run PFI 3 were analysed by XRD and SEM to determine phase relations. The residue is dominated by quartz and needle-like aggregates of chloritoid, phengite, epidote, and talc. Occasional large (up to 30 μm) blades of a Na–Mg sheet silicate, close to saponite in composition, also occur in the mineral aggregates and precipitated on the outer capsule wall. Accessory phases include <5 μm-sized grains of apatite, zircon, and rutile, and possibly submicron grains of U-oxide. However, several grains of euhedral rutile up to 100 μm across were also found associated with quartz-and phengite-rich material that precipitated on the walls of the outer capsule. This indicates that significant fluid-assisted mass transfer had occurred within the capsule during the experiment. Only a few of the pyrope grains that were added to the starting mix to promote garnet growth have observable (~1–2 μm) discontinuous overgrowths of almandine-rich garnet. Therefore garnet is interpreted to be stable under these conditions, but garnet growth was inhibited by the low T of the run.

4.2.1.2. PFI 2 (650 °C, 2.2 GPa). There is no evidence of melting of the EPSM in run PFI 2, indicating that run conditions were subsolidus. However, as in run PFI 3, fluid-driven mass transport had caused precipitation of silica spheres with minor phengite and apatite on the walls of the large outer capsule. Major minerals of the EPSM residue contained within the inner capsule include quartz, phengite, epidote, amphibole, and chloritoid. The Na–Mg sheet silicate and talc present in run PFI 3 were not found in PFI 2 and we suggest that these phases may have reacted to form amphibole. Apatite, zircon, rutile and possibly U-oxide are again accessory minerals. All of the pyrope seeds are rimmed with almandine-rich garnet that is easily distinguishable in backscatter electron images (Fig. 4A). The pronounced growth of garnet is compensated by a marked decrease in the proportion of chloritoid compared to run PFI 3, indicating that chloritoid reacts to garnet with increasing T.

4.2.1.3. PFI 7 (675 °C, 2.2 GPa). Two types of residue were recovered from the inner capsule of run PFI 7. Small amounts of the residue were similar to the residue from run PFI 2, consisting of quartz, phengite, pyrope seeds with almandine-rich rims, and accessory chloritoid, zircon, epidote, and rutile. These residue materials have not undergone melting. By contrast, the only mineral phases present in the remainder of the residue are garnet (pyrope seeds and almandine-rich rims) and accessory kyanite, rutile, and zircon. These phases are set within a matrix material that could not be examined by SEM due to dissolution of the matrix during sample polishing. Analysis of exposed inclusions in quartz (see below) reveals that the matrix material is likely to be melt that did not form a stable glass during quenching. Comparisons of these residues to residues from runs PFI 4 and PFI 6 (Fig. 4) also indicate that the pelitic starting material had undergone partial melting in run PFI 7.

4.2.1.4. PFI 4 (700 °C, 2.2 GPa) and PFI 6 (750 °C, 2.2 GPa). Quenched rhyolitic glass occurs throughout the residue materials from experiments PFI 4 and PFI 6 (Fig. 4C,D,E), confirming that the water saturated solidus for the EPSM is below 700 °C at 2.2 GPa. Mineral phases are garnet, rutile, and trace zircon in PFI 4, and garnet, rutile, trace zircon, and trace monazite in PFI 6. Garnet grains from both runs include pyrope seed overgrown by thick (up to 20 μm) almandine-rich rims, as well as almandine-rich grains grown without a pyrope seed crystal. The almandine-rich garnets occasionally contain clusters of submicrometre zircon grains.

4.2.2. Subsolidus fluid compositions

4.2.2.1. Description of inclusions. Quartz from both PFI 3 (600 °C) and PFI 2 (650 °C) experiments contains abundant fluid inclusions in inclusion trails or as isolated inclusions (e.g., Fig. 3C,D). Most of the larger inclusions (>50 μm) are dark and contain vapour bubbles of varying size, indicating that these inclusions had suffered decrepitation during quenching. This inclusion type was avoided during chemical analysis. Most other inclusions are 5–30 μm in size, translucent, and lack a vapour phase. However, these inclusions usually contain tiny daughter crystals of unknown composition. The inclusions in PFI 3 tend to contain one or more tabular daughter crystals (Fig. 3C), whereas inclusions in PFI 2 contain fine clusters of needle-like daughter crystals that have grown on the inclusion walls (Fig. 3D). These inclusions were targeted during LA-ICPMS analysis as they are deemed

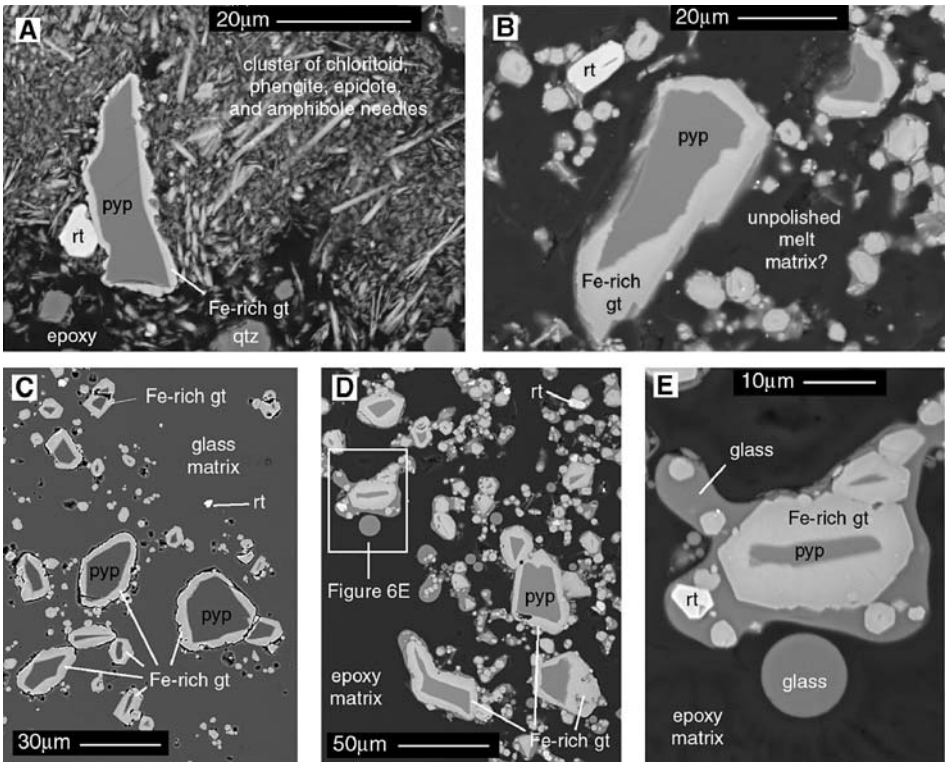

Fig. 4. Backscattered SEM images of EPSM residues from experimental runs. A. PFI 2 (650 °C) residue consisting of rutile, quartz, garnet (pyrope seed with almandine-rich overgrowth) set in a fine-grained matrix of chloritoid, phengite, amphibole, and epidote. B. PFI 7 (675 °C) melted residue consisting of rutile and pyrope seeds with almandine-rich overgrowths set in a poorly quenched melt matrix. C. PFI 4 (700 °C) melted residue of rutile and pyrope seeds with almandine-rich overgrowths set in a quenched glass matrix. D, E. PFI 6 (750 °C) residue of rutile and pyrope seeds with almandine-rich overgrowths coated with quenched glass.

to be representative samples of the fluid present at experimental run conditions.

4.2.2.2. Quantification of fluid inclusions. Quantification of element concentrations in the fluid inclusions by LA-ICPMS analysis requires internal standardization against an element of known concentration in the fluid. Analysis of major elements (e.g., K) in selected inclusions was attempted using proton-induced X-ray emission (PIXE), but element concentrations proved too low to be determined by this technique. Therefore, to constrain the concentration of an element for internal standardization, the maximum and minimum concentration of a range of elements in the fluid was bracketed using mass-balance considerations and the composition of fluid extracted from the capsules after quenching.

The composition of the extracted fluid (Table 4) provides minimum concentrations of elements in the fluid at run conditions, as the extracted fluid is likely to be depleted due to saturation in mineral phases during quenching. Consideration of mass loss from the pelite residue after experiment completion may be used to constrain maximum fluid concentrations. The comparison of the residue composition (Table 4) with the starting material (Table 1) shows that considerable amounts of Cs (90%), Na_2O (70–75%) and K_2O (30–40%) have been lost from the residue during the subsolidus experiments. If the full amount of these elements that are not accounted for in the residue has been dissolved in the fluid, then the concentration can be calculated by the following mass balance:

$$C_i(\text{fluid}) = [C_i(\text{EPSM}) - C_i(\text{residue})]/X$$

where X is the starting mass ratio of fluid to EPSM (Table 2) and C_i is the element concentration. In principle, the design of our experiments with high X values is ideal for such an approach. However, the precipitates of phengite, and Na-mica found on the wall of the outer capsule (Fig. 1) verify that hydrothermal mass transport and deposition of Na and K takes place during the experiments. Therefore, these mass balance calculations place constraints on the maximum elemental concentrations in the fluid, as the effect of mineral dissolution/

Table 4
Major and trace element concentrations of EPSM residues from subsolidus experiments, calculated maximum element concentrations in the fluid and composition of extracted from the capsules after run quenching (minimum fluid composition)

Run no.	PFI 3	PFI 2		PFI 3	PFI 2	PFI 3	PFI 2
Temp. (°C)	600	650		600	650	600	650
	Residue	Residue		Max. fluid concentration	Max. fluid concentration	Min. fluid concentration	Min. fluid concentration
EDS (wt.%)			*Calculated (ppm)*			*Solution ICP-AES (ppm)*	
SiO_2	73.70	72.87	Si	nr	nr	–	–
TiO_2	0.77	0.75	Ti	nr	nr	–	–
Al_2O_3	12.83	13.16	Al	2430	2500	112	30
FeO	5.28	4.90	Fe	nr	nr	–	–
MgO	3.11	2.94	Mg	nr	200	20	24
CaO	2.29	2.25	Ca	210	290	75	27
Na_2O	0.77	0.66	Na	3000	3800	1869	2733
K_2O	1.79	1.96	K	2000	2100	298	450
Sum	100.54	99.49					
LA ICP-MS (ppm)			*Calculated (ppm)*			*Solution ICP MS (ppm)*	
			In*			1026	1010
P	783	833	P	141	156	–	–
Sc	50	51	Sc	1.3	1.4	–	–
Ti	3383	3191	Ti	54	117	–	–
Mn	624	634	Mn	40	45	–	–
Rb	74	103	Rb	34	33	1.13	2.08
Sr	155	142	Sr	13	20	1.34	0.83
Y	54	57	Y	1.3	0.8	0.04	<0.004
Zr	199	201	Zr	0.7	0.3	–	–
Nb	46	48	Nb	2.4	2.4	–	–
Cs	20	26	Cs	50	58	2.49	4.56
Ba	764	933	Ba	92	65	4.41	0.67
La	127	131	La	8.0	8.6	0.13	0.03
Ce	53	53	Ce	3.4	4.0	–	–
Nd	47	49	Nd	2.9	3.0	–	–
Sm	53	59	Sm	3.0	1.9	–	–
Eu	48	50	Eu	3.0	3.1	–	–
Gd	48	50	Gd	2.3	2.2	–	–
Dy	47	49	Dy	1.8	1.6	–	–
Er	49	52	Er	1.8	1.6	–	–
Yb	53	56	Yb	1.6	1.2	–	–
Hf	41	43	Hf	1.7	1.5	–	–
Ta	51	54	Ta	1.3	0.9	–	–
Pb	88	73	Pb	28	38	–	–
Th	211	218	Th	6.0	5.4	–	–
U	417	428	U	26	28	0.38	<0.01

Notes: See text for details of analytical techniques and calculation of maximum element concentrations in the fluid. Quenched solutions extracted from the experiments were diluted 1:100 and 1:1000 for ICP AES and ICP MS analyses respectively. * Prior to dilution, In was added to the solution at a nominal level of 1000 ppm to check instrument and dilution accuracy. nr = not resolvable.

precipitation by fluid cycling during the experiment cannot be accounted for. It is worth noting that there is a slight increase in the SiO_2 content in the residue when compared to the starting material, indicating that the residue gained some SiO_2 that was likely transported to the inner capsule by quartz solution-precipitation during the run. Immobile element concentrations (e.g., Zr, HREE) in the bulk residue and the EPSM starting material are similar (Tables 1 and 4), which indicates that residue mass was close to conservative during the experiments (i.e., Si addition was closely matched by 'mobile element' loss from the residue) and hence this process does not significantly influence the calculation of the maximum fluid concentration of K, Na, and Cs. Also pelite residues are contained within the inner silver capsule (Fig. 1), which is open to fluid interaction. However, only a small fraction of the fluid will be present within the inner capsule at any time, so contamination of the EPSM residue by crystals formed from the fluid on quenching is considered negligible.

Fluid major-element concentrations that are constrained to within an order of magnitude by these maximum and minimum techniques for both PFI 2 and PFI 3 are Na and K (Fig. 5). Potassium in the fluid is buffered by phengite in both experiments and phengite is expected to be stable in pelitic rocks throughout the eclogite-facies (Domanik and Holloway, 1996; Hermann and Green, 2001). The constraints on K contents in the fluid are between 300 and 2000 ppm for PFI 3 and between 450 and 2100 ppm for PFI 2 (Table 4). Therefore, we have chosen K concentrations of 1000 ppm and 1500 ppm as internal standards to quantify the fluid inclusion analyses in PFI 3 and PFI 2 respectively. These values are estimates of the K content of fluids, but are constrained by the calculated range in fluid compositions (Fig. 5) and are consistent with expected K solubility with T (Manning, 2004a). Importantly, the ranges of element concentrations in fluid inclusions quantified in this manner almost exclusively fall within the maximum and minimum concentration constraints for the fluid composition (Fig. 5), which further supports the K concentrations chosen for internal standardization.

4.2.2.3. Fluid compositions. The average fluid inclusion compositions are presented in Table 5. Silica contents of the fluids were calculated from data on silica solubility in H_2O (Manning, 1994), although these values are regarded as minimum values as silica solubility in Na–Al–Si bearing systems is expected to be significantly higher (Manning, 2004b). Relative errors for the fluid compositions are generally around 50% for most elements, although higher standard deviation values (up to 94%) are reported for some elements (e.g., U, Th). The high variance for these elements is largely due to low concentrations in the fluid inclusions which are approaching analytical detection limits, but may also be artefacts of the analytical techniques used, such as using long dwell times for measuring the short transient signal produced by fluid inclusion ablation (Pettke et al., 2000). Nonetheless, even considering all of these uncertainties in fluid composition, it is clear that the fluids are relatively dilute; a premise consistent with the small proportion of daughter phases in the fluid inclusions (Fig. 3C,D). Fluid compositions at 600 °C (PFI 3) and 650 °C (PFI 2) contain approximately 4.0 and 5.5 wt.% solutes respectively, most of which (predicted ~75%) is SiO_2. The fluids have similar concentrations for most elements except the 650 °C fluid contains significantly higher large-ion lithophile element (LILE; K, Na, Rb, Sr, Ba, Cs) and Al contents. Garnet-hosting elements Y, Gd, and Yb are higher in the 600 °C fluid, which is probably an artefact of sluggish garnet growth in the low-T run. Compared to the EPSM, the fluids have relatively high Cs and Na contents and very low La, Th, U, and Zr contents (Fig. 5). Normalized concentrations of Ba are significantly lower than other LILE. Relative concentrations of Nb are higher than Ti or Ta, (Fig. 6) leading to elevated Nb/Ta in the fluid compared to the EPSM.

4.2.3. Supersolidus fluid and melt compositions

Sections of the quartz chips recovered from experiment PFI 7 (675 °C) are crowded with large (~1 mm) interconnecting inclusions (Fig. 3E). The inclusions often contain a vapour bubble of varying size and fine

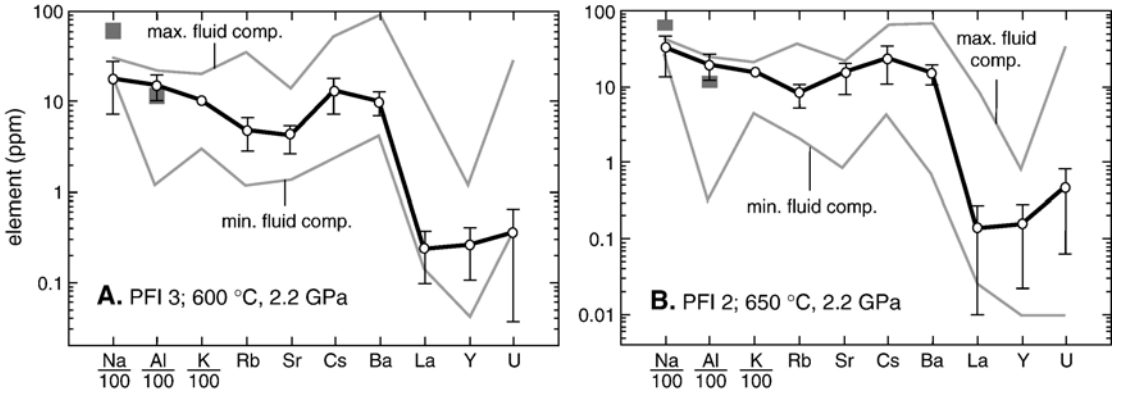

Fig. 5. Multi-element plots of fluid inclusion compositions and fluid composition constraints for (A) PFI 3 (600 °C) and (B) PFI 2 (650 °C). The upper grey line represents the maximum fluid composition as constrained from mass balance calculations and the lower grey line represents the minimum fluid composition as constrained by the composition of fluids extracted from the capsule after quenching. See text for details. The solid black line represents the average fluid inclusion composition using values of 1000 ppm K and 1500 ppm K as internal standards for PFI 3 and PFI 2 respectively. The error bars given on each element represents one standard deviation from the calculated fluid inclusion compositions, based on inclusion-to-inclusion analytical reproducibility. The dark grey rectangles for Na and Al represent concentrations in fluid released at the blueschist-eclogite transition, based on thermodynamic calculations of Manning (1998).

Table 5
Average element concentrations (ppm) of fluids from subsolidus experiments and calculated solid/fluid partition coefficients (D)

	Fluid composition (ppm)		Fluid composition (ppm)		D (solid/fluid) mass balance	D(solid/fluid) residue	D(solid/fluid) range	D(solid/fluid) mass balance	D(solid/fluid) residue	D(solid/fluid) range
Run no.	PFI 3		PFI 2		PFI 3	PFI 3	PFI 3	PFI 2	PFI 2	PFI 2
Temp. (°C)	600	1SD %	650	1SD %	600	600	600	650	650	650
Si*	15,500		22,000							
Al	1409	41	1930	38	**52**	48	34–91	**37**	36	26–62
Ca	764	48	772	78	**18**	21	11–41	**19**	21	9–98
Na	1735	58	2826	57	**6.5**	3.3	2.1–22	**3.0**	1.7	0.6–12
K	1000	0	1500	0	**19**	15	15–19	**12**	11	11–12
Ti	29	57	22	71	**120**	120	74–286	**160**	150	85–565
Rb	4.7	41	7.6	34	**43**	16	11–77	**26**	14	10–41
Sr	4.0	36	14	44	**49**	39	28–80	**12**	10	7–24
Y	0.26	59	0.15	85	**230**	210	131–558	**400**	380	205–2663
Zr	0.38	45	0.41	59	**530**	520	361–962	**490**	490	306–1198
Nb	0.61	43	0.71	45	**89**	76	53–159	**77**	68	47–142
Cs	13	44	23	53	**14**	1.5	1.1–29	**6.8**	1.1	0.7–19
Ba	10	31	15	30	**114**	77	59–167	**75**	62	48–108
La	0.23	59	0.14	93	**700**	550	347–1724	**1200**	930	485–16,700
Gd	0.81	43	0.37	79	**67**	59	41–121	**150**	134	75–743
Yb	0.73	61	0.31	78	**78**	73	45–206	**190**	180	101–876
Ta	0.37	40	0.32	63	**150**	140	98–252	**170**	170	104–478
Pb	1.3	57	1.8	63	–	**57**	36–132	–	**49**	30–132
Th	0.52	83	0.24	94	**450**	410	222–2688	**990**	910	468–16,500
U	0.35	90	0.44	86	1500	1190	627–15,200	1200	970	523–8633
Total solutes	~4.0		~5.5							

Notes: Fluid compositions represent the average fluid inclusion composition standardised on the basis of 1000 ppm and 1500 ppm K for PFI 3 and PFI 2 respectively. Errors given are one standard deviation in percentage. See text for details of method of partition coefficient (D) calculation. Bold values are preferred D values. U and Pb values are regarded as maximum and minimum values respectively, due to the possible formation of U-oxide in the pelite residues and Pb alloying with the silver capsule. * Si contents were calculated from Manning (1994), but are regarded as mimimum values for this system (Manning, 2004a). Total solutes are expressed as wt.% oxides.

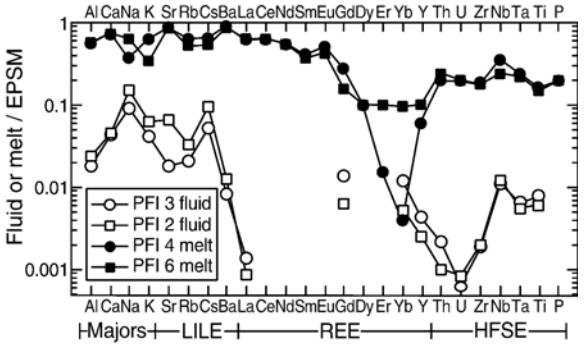

Fig. 6. EPSM normalised multi-element diagram of experimental fluid and melt compositions. Note, the fluids generally have element concentrations that are between 1 and 3 orders of magnitude lower than the melts. Data for many REE in the fluids are not presented as these elements were not analysed. EPSM values are in Table 1.

radiating clusters of quenched daughter phases. There is evidence of partial melting of the EPSM residue in PFI 7, although quenched melt could not be analysed from the residue, as discussed above. However, in some cases exposed inclusion cavities in quartz preserve thin rims of rhyolitic melt that could be polished and analysed for major elements by EDS. The compositions of the quenched melts are variable; some melts are relatively SiO_2 rich and Al_2O_3 poor, and others are Al_2O_3 and CaO rich and relatively SiO_2 poor (Table 6).

Quenched glass is preserved throughout the EPSM residues of experiments PFI 4 (700 °C) and PFI 6 (750 °C). The glasses from both experiments are homogenous with similar rhyolitic, peraluminous compositions. Low major element totals indicate that these glasses contain in excess of 10 wt.% H_2O components (Table 6). However, the quenched glass contains abundant vesicles indicating that the melt also exsolved fluid during quenching. Melt compositions are presented in Table 6 and Fig. 6, although the presented compositions are regarded as maximum concentration values as any exsolved fluid component cannot be constrained. Nonetheless, trace-element concentrations of both melts are lower than in EPSM largely due to the preserved high water contents of the melts. The melts are enriched in LILE, particularly Ba and Sr, compared to REE and high-field-strength elements (HFSE). REE patterns are LREE enriched and have positive Eu anomalies. HREE concentrations are significantly lower in the PFI 4 melt compared to PFI 6 melt. Both melts have higher Nb/Ta than the EPSM.

Inclusions trapped in the quartz chips from each of the runs were examined to assess if one or two liquid phases (fluid+melt) were present at run conditions. As with PFI 7, quartz chips in PFI 4 and PFI 6 are congested with large (0.1–1 mm) rectangular to quasi-rectangular inclusions (Fig. 3F). However, due to the extensive pelite melting of PFI 4 and PFI 6, we expect equilibrium conditions were rapidly reached in these experimental runs. The inclusions generally have vapour bubbles of varying size and usually contain complex clusters of quenched daughter phases (Fig. 3F,G). Inclusions cooled to below −50 °C on a fluid inclusion heating/freezing stage were observed to melt close to 0 °C during reheating. This result demonstrates that the inclusions consist mostly of aqueous fluid with a relatively small melt component.

Element concentrations in the inclusions from PFI 4 and PFI 6 could not be quantified from LA-ICPMS analyses, as the concentration of a reference element for

Table 6
Major (wt.%) and trace (ppm) element concentrations of quenched melt from experiments PFI 7, 4 and 6

Run no.	PFI 7 [5]	PFI 7 [7]	PFI 4 [9]	PFI 6 [7]
Temp. (°C)	675	675	700	750
SiO_2	80.65	65.79	73.43	71.12
TiO_2	0.03	0.04	0.10	0.14
Al_2O_3	7.18	12.38	8.64	8.84
FeO	bdl	0.03	0.54	0.37
MnO	0.10	bdl	0.02	0.02
MgO	0.05	0.05	0.40	0.53
CaO	2.20	4.05	1.84	1.89
Na_2O	2.12	2.25	1.00	1.61
K_2O	1.65	2.20	1.76	0.99
Total	93.98	86.79	87.73	85.51
P			289	281
Ti			578	513
Mn			92	48
Rb			138	115
Sr			186	195
Y			3.8	6.1
Zr			37	37
Nb			20	14
Cs			155	127
Ba			1086	1064
La			102	108
Ce			44	45
Nd			33	43
Sm			27	25
Eu			31	25
Gd			16	9.1
Dy			5.8	5.6
Er			0.85	5.4
Yb			0.24	5.5
Hf			13	13
Ta			13	13
Th			47	60
U			106	106

Note: Number in square brackets denotes number of analyses. Relative standard deviations are less than 10% for all trace elements presented, except for Yb (11%), Y (11%), Th (11%) and P (14%) in PFI 4.

internal standardization could not be constrained. Nonetheless, element ratios of inclusions were determined and allow evaluation of fluid and melt proportions based on comparison with fluid-melt mixing models (Fig. 7). Modelling of fluid-melt mixing was conducted using element ratios of the quenched glasses and fluid from PFI 2 as respective melt and fluid components. Experiment PFI 2 was conducted at lower temperatures and under subsolidus conditions. Therefore, strictly speaking the use of the fluid composition from PFI 2 is not appropriate for modelling fluid compositions at supersolidus conditions. However, temperature differences between experiment PFI 2 and experiments PFI 4 and PFI 6 are only 50 and 100 °C respectively, so for the purposes of determining fluid phase relations using element ratios that vary over several log units (Fig. 7), we regard the PFI 2 fluid composition to be generally representative of the fluid phases in the supersolidus experiments. Examining element ratios that are strongly fractionated by fluid and melt also minimizes uncertainties related to the representative modelled compositions. The data for populations of inclusions from both

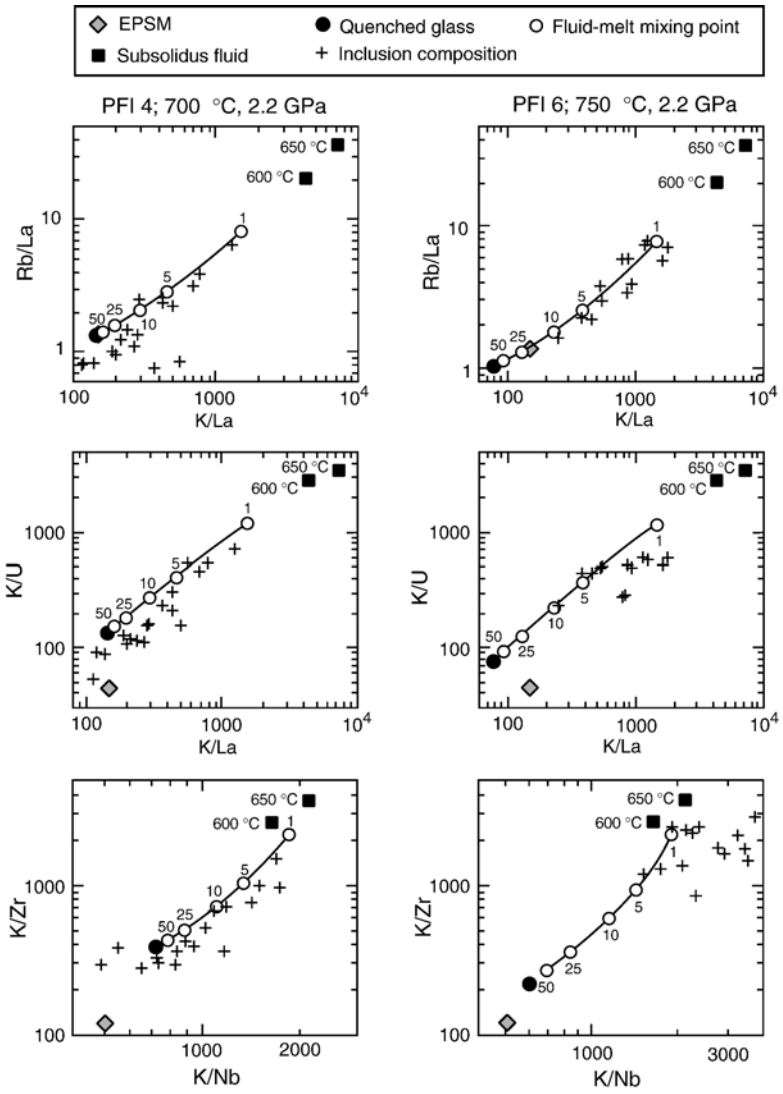

Fig. 7. Element ratio plots distinguishing fluid and melt components in inclusions from PFI 4 (700 °C) and PFI 6 (750 °C). Mixing lines between quenched glass and PFI 2 fluid compositions are also plotted with numbers corresponding to melt-fluid mixing ratios of 50=50:50, 25=25:75, 10=10:90, 5=5:95, and 1=1:99. The scatter of data for the inclusions from PFI 4 and PFI 6 indicate that the inclusions contain variable proportions of fluid and melt. In this case the inclusions represent random mixtures of fluid and melt and hence fluid and melt coexisted as immiscible phases at run conditions. See text for further details.

experiments clearly show that the inclusions have variable compositions. As discussed above, equilibrium conditions are expected for these experiments, so these variations are not regarded as artefacts of non-equilibrium conditions, Instead, the variations are consistent with varying proportions of melt and fluid (Fig. 7). The modelled mixing trends indicate that most of the inclusions contain in excess of 50% hydrous fluid in PFI 4 and 90% hydrous fluid in PFI 6, which is consistent with the heating/freezing observations. More importantly, these results show that the inclusions represent random mixtures of fluid and melt that were trapped in quartz during the experiments. Therefore, two coexisting immiscible liquid phases (melt+fluid) were present at run conditions for both PFI 4 and PFI 6.

The composition of fluids coexisting with melt in PFI 4 and PFI 6 could not be precisely constrained. However, based on normalised melt compositions (Fig. 6) and element ratios presented in Fig. 7 the fluids are expected to have contained relatively high Cs, Rb, Na, and K contents.

4.3. Element partitioning

4.3.1. Solid/fluid

Element partitioning between bulk solid residue and subsolidus fluid was calculated using two methods. The first method, labelled the residue method, is simply the ratio of the extrapolated subsolidus fluid composition to the analysed EPSM residue composition (Table 4). Partition coefficients were calculated by the second method (mass-balance method) using the following formula;

$$\text{Solid/fluid partition coefficient } (D) = \frac{C_i \text{ EPSM} - X(C_i \text{ fluid})}{C_i \text{ fluid}}$$

where X is the starting mass ratio of fluid to EPSM (Table 2) and C_i is the element concentration. As Pb alloys with the capsule during the experiments, only the residue method was used to calculate Pb partitioning. Calculated partition coefficients are given in Table 5.

Partition coefficients calculated using the residue method are potentially inaccurate, as this method does not account for mineral precipitation on the capsule walls during the experiments. The precipitated alkali sheet silicates on the capsule walls of both PFI 3 and PFI 2 explains the significantly lower partition coefficients calculated for Na, Rb, and Cs using the residue method (Table 5, Fig. 8). Nonetheless, the partition coefficients produced using the two methods are remarkably similar for all other elements, indicating that most elements are not significantly affected by fluid transport and precipitation during the experiments. Furthermore, the correspondence of the datasets reinforces the overall accuracy of the methods used to quantify fluid compositions and hence the calculated partitioning values. In particular, the close correspondence of immobile

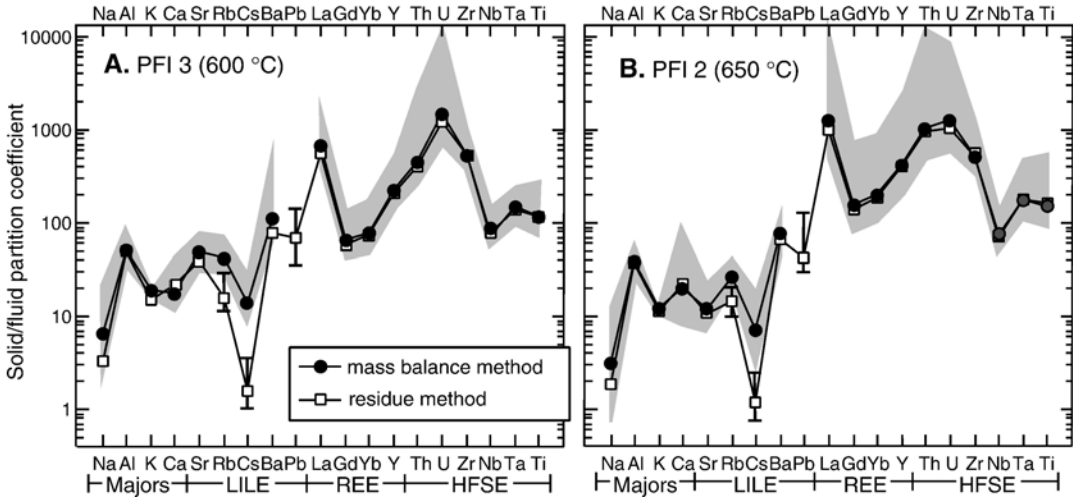

Fig. 8. Calculated solid/fluid partition coefficients for subsolidus fluid from experiments (A) PFI 2 (600 °C) and (B) PFI 3 (650 °C). The grey fields represent the total range of partitioning values calculated when including errors on the determined fluid compositions (Table 5). The ranges of values calculated by the mass balance and residue method overlap for all elements except Rb, Cs and Pb. Therefore separate error ranges for Rb, Cs and Pb calculated using the residue method are given as error bars. Partitioning data for Pb and U are regarded as maximum and minimum values respectively, due to Pb alloying with the capsule and possible formation of U-oxides in the pelite residues. See text for details on the methods used for partition coefficient calculation.

element partitioning values (e.g., Zr) supports our assumption of mass conservation in the pelite residue for constraining fluid compositions (see 'Quantification of fluid inclusions'). Partition coefficients calculated using the mass-balance method are preferred (Table 5). It should be noted that the solid/fluid partitioning data for U is regarded as a maximum value, as U-oxides are most likely present in the residue of the subsolidus experiments. These U-oxides probably form due to the high initial U content of the EPSM starting material (Table 1) and hence, U content of the fluid remained buffered during the experiments.

Examination of the partitioning data reveals that all elements preferentially partition into the solid residue rather than the fluid at subsolidus conditions (Table 5; Fig. 8). The effect of T over the range of investigated experimental conditions does not dramatically change the partitioning behaviour, although the solid/fluid partitioning of Cs, Rb, Na, and Sr decreases slightly with increasing T. In particular, Sr solubility increases with respect to other elements with increasing T. Overall, Na and Cs are the most fluid compatible elements, followed by K, Ca, Rb, and Sr. Elements that strongly partition into the solid residue are La, Th, and Zr. Partition coefficients for the garnet-hosting elements Gd, Yb, and Y are considered to be minimum values due to the sluggish garnet growth in the ESPM residues. Barium and Pb have similar partition coefficient to Nb, Ti, and Ta, and hence are much more compatible in the solid than other LILE. Niobium is slightly more compatible in the fluid than Ti or Ta.

4.3.2. Melt/fluid partitioning

Despite the recognition that fluid and melt coexisted in experiments PFI 4 and PFI 6, the fluid compositions from these runs could not be quantified and hence precise melt/fluid partition coefficients cannot be calculated. From petrographic observations, it is likely that the EPSM underwent extensive (~90%) melting to leave a residue of only garnet, rutile, and accessory zircon (±monazite). Therefore, rough constraints on partitioning for some elements can be made using the composition and proportion of melt and starting material and the volume of the fluid phase. Estimated partition coefficients for melt/fluid are likely to be 5–10 for K, Rb, and Cs, and ~50 for Sr and Ba.

5. Discussion

5.1. Phase relations in subducted pelitic rocks

It is well recognized that accurate experimental modelling of phase relations under subduction-zone conditions is difficult to accomplish (e.g., Forneris and Holloway, 2003). The relatively low T conditions inhibit growth of equilibrium mineral assemblages and may allow persistence of metastable phases. The experiments conducted in this study were designed to minimize metastable mineral growth by using a synthetic homogenous starting material, using pyrope crystals to seed garnet growth, using high fluid/solid ratios, and conducting long duration runs. The mineral assemblage formed in the experiments (garnet, quartz, phengite, epidote, chloritoid, zircon, rutile, apatite, ±talc, ±amphibole) is comparable with mineral assemblages predicted by phase equilibria and found in natural samples of eclogite-facies pelites (Poli and Schmidt, 2002; Spandler et al., 2003). An exception is the Na–Mg sheet silicate (saponite) in PFI 3 (600 °C), which, based on textural and geochemical grounds, is expected to be metastable and probably reacted out to form stable amphibole at higher T (650 °C). Na-rich sheet silicates of similar composition have been described from Na-amphibole synthesis studies conducted under similar P–T conditions (e.g., Pawley, 1992).

Recent work has shown that the trace-element inventory of eclogite-facies pelitic rocks is controlled by garnet (HREE, Y), rutile (Nb, Ta), epidote (REE, Sr, Th, Pb), zircon (Zr, Hf), phengite (LILE), and apatite (REE, P, Sr) (Hermann and Green, 2001; Spandler et al., 2003). All of these phases are present in the subsolidus experiments, so the trace-element composition of the fluids in the subsolidus experiments was controlled by an equilibrium mineral assemblage. The sluggish growth of garnet in experiment PFI 3 (600 °C) may be the cause of the high Yb, Gd, and Y contents (relative to La) of the fluids analysed from this experiment.

The presence of melt and melted residue together with unmelted residue in experiment PFI 7 indicate that conditions were close to the water-saturated (wet) solidus. The heterogeneous nature of the EPSM residue in PFI 7 may be due to slight (<10 °C) T gradients that may have existed in the capsule. Therefore, the wet solidus at 2.2 GPa is interpreted to be at 675 °C (±10 °C). The variable composition of the melt in the melted residue indicates that melting was non-equilibrium. Similar heterogeneities in melt compositions from close to the wet solidus were also found in an experimental study of high-P pelite melting by Nichols et al. (1996). The kyanite in the melted residue is suggested to be a product of incongruent melting of aluminous minerals such as phengite or epidote. By contrast, melt and residues produced in experiments at 700 and 750 °C are homogenous.

Nichols et al. (1994) defined the wet solidus for natural red clay at close to 650 °C at 2.0 GPa. These conditions are consistent with our results and the

experimentally determined wet solidus for granitic rocks (Stern and Wyllie, 1973; Huang and Wyllie, 1981). By contrast, Johnson and Plank (1999) determined the wet solidus of metalliferous pelagic clay to be 775 °C at 2.0 GPa. This difference in the location of the solidus is likely to be due to differences in bulk compositions of the starting materials used (Nichols et al., 1996), and possible lack of detection of melt or loss of fluid from the low T experiments of Johnson and Plank (1999), as suggested by Schmidt et al. (2004). The starting material used in this study was modelled on the composition of terrestrial sediments, which are the major source of trace elements in subducting sedimentary columns (Plank and Langmuir, 1998). Therefore, the determined position of the wet solidus is important for understanding element recycling through subduction zones.

A fundamental advantage of the experimental technique employed in this study is that samples of experimental fluids are trapped and isolated as inclusions in quartz at run conditions. Subsequent observation and analysis of these inclusions in the supersolidus experiments (PFI 4 and 6) has confirmed that coexisting fluid and melt were present at least 75 °C above the wet solidus at 2.2 GPa. It is noteworthy that the scatter in element ratios measured from the supersolidus inclusions (Fig. 7) decreases with increasing T. This feature may be a consequence of the progressive merging of fluid and melt compositions with increasing T approaching the closing of the two-phase field (Bureau and Keppler, 1999). Nonetheless, the presented data indicate that the second critical end-point for pelitic rocks is well above 2.2 GPa.

The high fluid/EPSM ratio used in our experiments (Table 2) produced very high degrees (~90%) of melting in runs conducted above the wet solidus. The melts examined in this study were not completely mineral buffered (e.g., no epidote or mica in the residue) and thus may have limited applicability to conditions of sediment melting in subduction zones. However, the EPSM has similar major element and Ti and Zr contents to pelitic sediments (Table 1), so the presence of rutile, zircon and garnet in the residue demonstrates that these phases may remain stable in subducted sedimentary rock even under extreme melting conditions. Rutile, zircon and garnet are the primary hosts for Ti, Nb, Ta, Zr, Hf, and HREE in high-P rocks (Hermann, 2002; Zack et al., 2002; Rubatto and Hermann, 2003; Spandler et al., 2003), which accounts for the relatively low HREE and HFSE content of the melt from PFI 4 and PFI 6 (Fig. 6). Consequently, high degrees of melting in the slab are likely to cause pronounced trace-element fractionation leaving an HFSE- and HREE-enriched residue.

5.2. Composition of subsolidus fluid in subduction zones

It is often assumed that aqueous fluid released from subducting rocks have an important role in elemental recycling through subduction zones, but as yet the compositions of such fluids are poorly known. The accuracy of our determined fluid compositions can be evaluated by comparison with expected fluid compositions determined from previous experimental and thermodynamic studies and from data from natural samples. The Na and Al contents of eclogite facies fluid calculated from thermodynamic properties (Manning, 1998) are remarkably similar to the Na and Al contents of our experimental fluids, as shown in Fig. 5. The LREE, Ti and Zr content of the fluids are also consistent with the expected low Ce contents (0.43 ppm) of allanite-saturated fluids at 600 °C (Hermann, 2002), and calculated Ti and Zr contents of eclogite-facies fluids (Fig. 9; Green and Adam, 2003; Rubatto and Hermann, 2003; Audétat and Keppler, 2005). In particular, the Ti data correspond very well with the expected Ti solubility in albite-bearing hydrous fluid, as reported by Antignano and Manning (2005) and Audétat and Keppler (2005). Collectively, these data comparisons confirm the accuracy of the internal standardization of the fluid inclusion data. Our fluid compositions have low solute contents (~5 wt.%), and it is expected that fluids derived from mafic rocks at similar P–T conditions in the slab will be similarly dilute (e.g., Green and Adam, 2003; Manning, 2004a)

All of our EPSM experiments contain residual rutile and zircon, so the Ti and Zr contents of the fluids and melts can be directly compared to data from other rutile and zircon saturated experiments (Fig. 9). The Ti and Zr contents of the supersolidus melts are consistent with concentrations expected for low-T rhyolite. Ti solubility in pure H_2O is around an order of magnitude lower than for solute-bearing aqueous fluids, whereas the Ti contents of rutile-saturated melts are about an order of magnitude higher than aqueous fluids at the same temperature. A similar trend is observed for Zr contents of zircon saturated melts and fluids.

Our partitioning data indicate that all trace elements are more compatible in eclogite-facies pelite than in a coexisting hydrous fluid phase. This result conflicts with data obtained from diamond trap experiments of Johnson and Plank (1999), who reported many elements partitioning in favour of the fluid phase. Johnson and Plank (1999) conducted experiments under similar P and T conditions to our experiments, but reported solid/fluid partition coefficients for a range of elements that are between 1 and 3 orders of magnitude lower than the partition coefficients reported in this study. We attribute

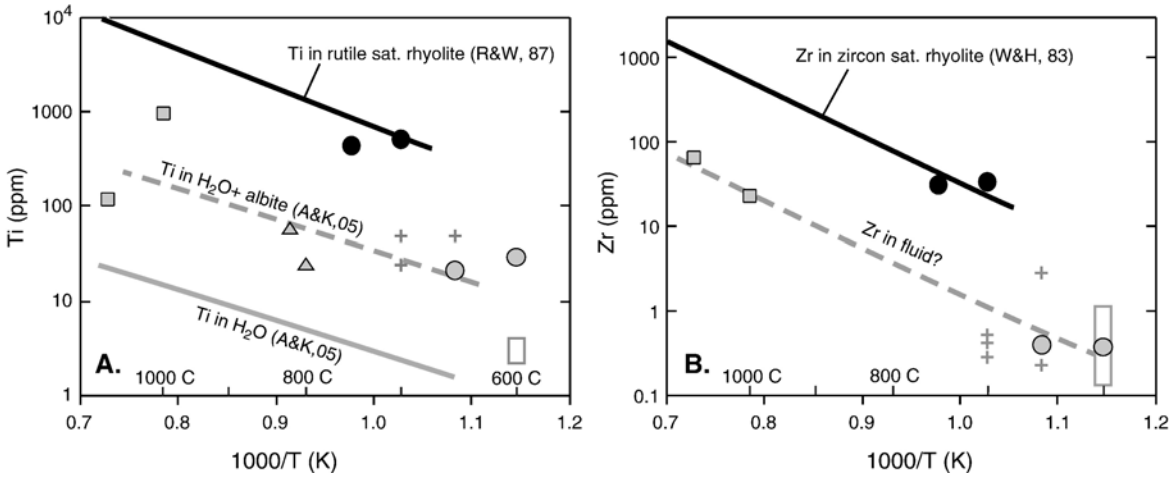

Fig. 9. A. Ti content of high-P (2–3 GPa) rutile saturated fluids and rhyolitic melts. B. Zr content of high-P (2–3 GPa) zircon saturated fluids and rhyolitic melts. The grey and black symbols and trends are data for fluids and melts respectively. Modelled trends for Ti and Zr saturated rhyolitic melts (FM=0.5, P=2.2 GPa) are from Ryerson and Watson (1987) and Watson and Harrison (1983) respectively. Ti in fluid trends are from Audétat and Keppler (2005) (P=2.2 GPa). Data sources; circles — this study; crosses — Green and Adam (2003 normalised to 10% total solutes in the fluid); open rectangles — Rubatto and Hermann (2003); squares — peridotite fluid from Ayers et al. (1997); triangles — albite-bearing hydrous fluid from Audétat and Keppler (2005).

these significant differences to problems associated with the experimental technique used by Johnston and Plank. Firstly, processes of mineral dissolution and reprecipitation in the diamond trap cannot be accounted for. As discussed above, these processes are invoked to explain the mineral precipitates on the wall of the outer silver capsule in our experiments. In long-duration diamond trap experiments this may lead to concentration of mineral precipitates in the diamond trap. Secondly, it is likely that some of the fine-grained (<10 μm) residual material physically intruded into the diamond trap (50 μm grainsize) during the experiments of Johnson and Plank (1999). Bulk analysis of the diamond trap contaminated by residue material or mineral precipitates will produce erroneous calculated partition coefficients that approach 1. This is consistent with the partition coefficients of Johnson and Plank (1999) that span a small range from 0.5 to 4 for most elements.

The problems outlined above are not relevant to the fluid compositions presented here as we have directly analysed samples of fluid that was trapped in quartz at run conditions and was buffered by the appropriate high-P mineral assemblage in the solid residue. The composition of these fluids are well constrained by mass balance (Fig. 5) and compare favourably with other studies that report on high-P fluid compositions. Therefore, our experiments model fluid-rock interactions in subducted sedimentary rocks and hence, have important implications for fluid and element transfer from subducting slabs and the generation of arc magmas.

5.3. Implications for element recycling through subduction zones

Isotopic and geochemical studies of modern arc systems indicate that subducted sediments provide the major proportion of many elements to arc magmas (e.g., Plank and Langmuir, 1993), yet there is debate as to whether hydrous fluids or melts (or both) are the primary agents responsible for fluxing volatile and trace elements out of the slab (e.g., Class et al., 2000; Elliott, 2003). Identifying the agents (melt or fluid) is not only critical to the generation of arc magmatism, but may also place constraints the thermal state of subduction zones and element recycling through the Earth.

Eclogite-facies mafic and pelitic rocks can have similar trace-element-hosting mineral assemblages (Spandler et al., 2003). Therefore, the experimental results presented in this paper can be used to model slab processes under eclogite-facies conditions at fore-arc depths (~70 km). Mineral dehydration during progressive subduction-zone metamorphism is widely regarded to be the major source of water for slab fluids, slab melts, and ultimately arc magmas. Sedimentary rocks are expected to release around 1 wt.% as H_2O during blueschist to eclogite-facies metamorphism (Spandler et al., 2003). The trace-element loss accompanying this fluid release can be evaluated using the composition of fluid in equilibrium with pelite under eclogite-facies conditions (Table 5). The degree of element loss is calculated to be less than 0.1% of the original composition for almost

all elements (Fig. 10). The highest losses are for Na and Cs, but even these elements are only depleted by around 0.3 and 0.1% respectively. These very low levels of element loss during metamorphism are directly comparable to the calculated element losses from eclogite-facies mafic and pelitic rocks from New Caledonia (Spandler et al., 2004a), and confirm earlier assertions that subducting rocks may preserve the chemical characteristics of their protolith at least up to eclogite facies (Chalot-Prat et al., 2003; Spandler et al., 2004b). The lack of element depletion to fluids under these conditions indicates that trace elements in the slab can be efficiently transported to sub-arc depths (3–5 GPa). Moreover, this implies that zones of extreme fluid-induced element depletion in blueschist and eclogite-facies rocks (e.g., Breeding et al., 2004; John et al., 2004) must require very large fluid fluxes and hence represent significant fluid channelways in the slab.

Kessel et al. (2005) report on partitioning of trace elements between K-free mafic eclogite and fluid at 4–6 GPa. By contrast, there are no data on element solubility in aqueous fluids in equilibrium with pelite at P conditions higher than those examined here, so overall the composition of fluids present at sub-arc depths remain poorly constrained. Element solubilities are expected to increase somewhat with increasing P and T conditions (Bebout et al., 1999; Manning, 2004a; Kessel et al., 2005), but we expect that aqueous fluids are unlikely to become distinctly solute rich while remaining buffered by an eclogite-facies mineral assemblage of garnet, omphacite, phengite, allanite/epidote, rutile, and zircon (±apatite or monazite). From experimental studies

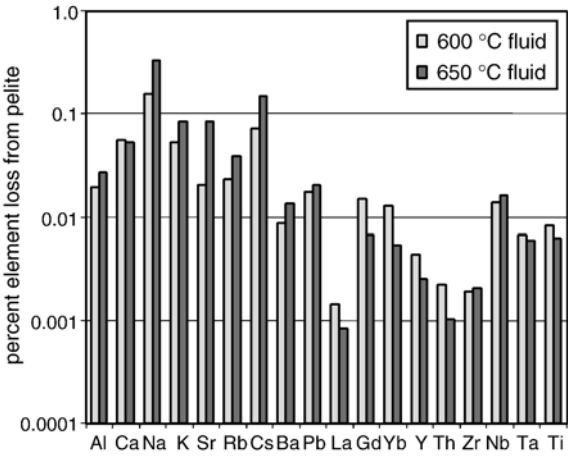

Fig. 10. Calculated percentage of element loss caused by dehydration and extraction of 1 wt.% of fluid from pelite at 2.2 GPa, 600 °C and 2.2 GPa, 650 °C. Note, the degree of element loss is very low (~0.1% or less).

and natural samples of UHP rocks, such a mineral assemblage may be stable in mafic and pelitic rocks to over 4.0 GPa and 800 °C (Hermann, 2002; Compagnoni and Rolfo, 2003).

Assuming element solubility in eclogite-facies aqueous fluids does not increase dramatically during subduction from fore-arc (2.2 GPa) to sub-arc (3–5 GPa) depths, then aqueous fluids liberated from the slab at sub-arc depths are likely to be relatively dilute. These fluids would have a limited capacity to transport elements from the slab into the overlying mantle wedge. From our experiments and the work of Nichols et al. (1994, 1996), it is expected that metasedimentary rocks will undergo melting in the presence of a fluid at or above 700 °C. At sub-arc depths fluids may be sourced from dehydration of serpentinite in the underlying subducted oceanic lithosphere or overlying hydrated mantle wedge (Ulmer and Trommsdorff, 1999). The hydrous melts produced are likely to have element concentrations that are significantly greater that coexisting aqueous fluids (e.g., Fig. 9) and therefore will be highly effective agents for transferring elements from the slab into the mantle wedge. However, this circumstance requires deep subduction of sedimentary rocks as well as slab surface temperatures of 700 °C or higher at sub-arc depths (3.0–5.0 GPa); conditions which are currently the subject of debate (e.g., Kincaid and Griffiths, 2004; Stern et al., 2006). Furthermore, the importance of serpentinite dehydration fluid in subduction-zone element recycling remains largely unknown (Scambelluri et al., 2004). For a more comprehensive understanding of deep subduction processes it is clear that further experimental work is required to constrain fluid and melt compositions at sub-arc depths.

6. Conclusions

Using innovative experimental techniques, we have performed hydrothermal experiments at 2.2 GPa on a synthetic pelite starting material in order to model phase relations and fluid compositions in deeply subducted sedimentary rocks. By analysing fluid inclusions trapped in quartz during the experiments, subsolidus fluid compositions were determined and solid/fluid partition coefficients for a range of major and trace element were calculated. Although fluids preferentially partition LILE over REE or HFSE, all elements partition in favour of the solid at 600–650 °C. At 2.2 GPa, the H_2O-saturated solidus for the pelitic starting material is located at approximately 675 °C. Melt and fluid coexist above the solidus at least up to 750 °C, limiting the critical curve for pelitic rocks to higher T at 2.2 GPa.

Our data are used to show that subsolidus fluids released during subduction-zone metamorphism up to eclogite-facies are too dilute to significantly alter the trace element content of subducting pelite. This premise allows efficient transport of trace elements to sub-arc depths. Such aqueous fluids are not likely to be effective agents for transporting trace elements, which indicates that element recycling through subduction zones may involve highly complex fluid-rock interaction processes including fluid flux melting of metasedimentary rocks.

Acknowledgements

This research was supported by the Australian Research Council. We thank Bill Hibberson and Dean Scott for technical support. Reviews by Craig Manning and Stefano Poli and comprehensive editorial work by Thomas Pettke greatly improved the manuscript.

References

Allan, M.M., Yardley, B.W.D., Forbes, L.J., Shmulovich, K.I., Banks, D.A., Shepherd, T.J., 2005. Validation of LA-ICP-MS fluid inclusion analysis with synthetic fluid inclusions. Am. Mineral. 90, 1767–1775.

Antignano, A., Manning, C.E., 2005. Rutile solubility in H_2O–$NaAlSi_3O_8$ fluids at high T and P: implications for HSFE mobility in subduction zones. Eos Trans. AGU 86 (52) (Fall. Meet. Suppl., Abstract V31C-0620).

Audétat, A., Keppler, H., 2005. Solubility of rutile in subduction zone fluids, as determined by experiments in the hydrothermal diamond anvil cell. Earth Planet. Sci. Lett. 232, 393–402.

Ayers, J.C., Dittmer, S.K., Layne, G.D., 1997. Partitioning of elements between peridotite and H_2O at 2.0–3.0 GPa and 900–1100 °C, and application to models of subduction zone processes. Earth Planet. Sci. Lett. 150, 381–398.

Bebout, G.E., Ryan, J.G., Leeman, W.P., Bebout, A.E., 1999. Fractionation of trace elements by subduction-zone metamorphism; effect of convergent-margin thermal evolution. Earth Planet. Sci. Lett. 171, 63–81.

Bose, K., Ganguly, J., 1995. Quartz-coesite transition revisited: Reversed experimental determination at 500–1200 °C and retrieved thermochemical properties. Am. Mineral. 80, 231–238.

Breeding, C.M., Ague, J.J., Bröcker, M., 2004. Fluid-metasedimentary rock interactions in subduction-zone mélange: Implications for the chemical composition of arc magmas. Geology 32, 1041–1044.

Brodholt, J.P., Wood, B.J., 1993. Simulations of the structure and thermodynamic properties of water and high pressures and temperatures. J. Geophys. Res. 98, 519–536.

Brodholt, J.P., Wood, B.J., 1994. Measurement of the PVT properties of water to 25 kbars and 1600 °C from synthetic fluid inclusions in corundum. Geochim. Cosmochim. Acta 58, 2143–2148.

Brown, P.E., Hagemann, S.G., 1995. MacFlinCor and its application to fluids in Archean lode-gold deposits. Geochim. Cosmochim. Acta 59, 3943–3952.

Bureau, H., Keppler, H., 1999. Complete miscibility between silicate melt and hydrous fluids in the upper mantle: experimental evidence and geochemical implications. Earth Planet. Sci. Lett. 165, 187–196.

Chalot-Prat, F., Ganne, J., Lombard, A., 2003. No significant element transfer from the oceanic plate to the mantle wedge during subduction and exhumation of the Tethys lithosphere (Western Alps). Lithos 69, 69–103.

Class, C., Miller, D.M., Goldstein, S.L., Langmuir, C.H., 2000. Distinguishing melt and fluid subduction and components in Umnak volcanics, Aleutian Arc. Geochem. Geophys. Geosyst. 1 (Art. no. 1999GC000010).

Compagnoni, R., Rolfo, F., 2003. UHPM units in the Western Alps. In: Carswell, D.A., Compagnoni, R. (Eds.), Ultrahigh Pressure Metamorphism. EMU Note. Min., vol. 5. Eötvös University Press, Budapest, pp. 13–49.

Domanik, K.J., Holloway, J.R., 1996. The stability and composition of phengitic muscovite and associated phases from 5.5 to 11 GPa; implications for deeply subducted sediments. Geochim. Cosmochim. Acta 60, 4133–4150.

Elliott, T., 2003. Tracers of the slab. In: Eiler, J. (Ed.), Inside the Subduction Factory. Geophys. Mon., vol. 138. American Geophysical Union, Washington, DC, pp. 23–45.

Forneris, J.F., Holloway, J.R., 2003. Phase equilibria in subducting basaltic crust: implications for H_2O release from the slab. Earth Planet. Sci. Lett. 214, 187–201.

Green, T.H., Adam, J., 2003. Experimentally-determined trace element characteristics of aqueous fluid from partially dehydrated mafic oceanic crust at 3.0 GPa, 650–700°C. Eur. J. Mineral. 15, 815–830.

Green, T.H., Ringwood, A.E., Major, A., 1966. Friction effects and pressure calibration in a piston-cylinder apparatus at high pressure and temperature. J. Geophys. Res. 71, 3589–3594.

Günther, D., Audétat, A., Frischknecht, R., Heinrich, C.A., 1998. Quantitative analysis of major, minor and trace elements in fluid inclusions using laser ablation-inductively coupled plasma mass spectrometry. J. Anal. At. Spectrom. 13, 263–270.

Haar, L., Gallagher, J.S., Kell, G.S., 1984. NBS/NRC Steam Tables, Thermodynamic and Transport Properties and Computer Programs for Vapour and Liquid States of Water in SI Units. Hemisphere Publishing, New York.

Hack, A.C., Mavrogenes, J.A., 2006. A cold-sealing capsule design for fluid inclusion synthesis and other hydrothermal experiments in a piston-cylinder apparatus. Am. Mineral. 91, 203–210.

Hawkesworth, C.J., Gallagher, K., Hergt, J.M., McDermott, F., 1993. Mantle and slab contributions in arc magmas. Annu. Rev. Earth Planet. Sci. 21, 175–204.

Heinrich, C.A., Pettke, T., Halter, W.E., Aigner-Torres, M., Audétat, A., Günther, D., Hattendorf, B., Bleiner, D., Guillong, M., Horn, I., 2003. Quantitative multi-element analysis of minerals, fluid and melt inclusions by laser-ablation inductively-coupled-plasma mass-spectrometry. Geochim. Cosmochim. Acta 67, 3473–3497.

Hermann, J., 2002. Allanite: thorium and light rare earth element carrier in subducted crust. Chem. Geol. 192, 289–306.

Hermann, J., 2003. Experimental evidence for diamond-facies metamorphism in the Dora–Maira massif. Lithos 70, 163–182.

Hermann, J., Green, D.H., 2001. Experimental constraints on high pressure melting in subducted crust. Earth Planet. Sci. Lett. 188, 149–168.

Huang, W.L., Wyllie, P.J., 1981. Phase relationships of S-type granite with H_2O to 35 kbar: muscovite granite from Harney Peak, South Dakota. J. Geophys. Res. 86, 10515–10529.

John, T., Scherer, E.E., Haase, K., Schenk, V., 2004. Trace element fractionation during fluid-induced eclogitization in a subducting slab: trace element and Lu–Hf–Sm–Nd isotope systematics. Earth Planet. Sci. Lett. 227, 441–456.

Johnson, M.C., Plank, T., 1999. Dehydration and melting experiments constrain the fate of subducted sediments. Geochem. Geophys. Geosyst. 1 (Art. no. 1999GC000014).

Kessel, R., Ulmer, P., Pettke, T., Schmidt, M.W., Thompson, A.B., 2004. A novel approach to determine high-pressure high-temperature fluid and melt compositions using diamond-trap experiments. Am. Mineral. 89, 1078–1086.

Kessel, R., Schmidt, M.W., Ulmer, P., Pettke, T., 2005. Trace element signature of subduction-zone fluids, melts and supercritical liquids at 120–180 km depth. Nature 437, 724–727.

Kincaid, C., Griffiths, R.W., 2004. Variability in flow and temperature within mantle subduction zones. Geochem. Geophys. Geosyst. 5 (Art. no. Q06002).

Liu, J., Bohlen, S.R., Ernst, W.G., 1996. Stability of hydrous phases in subducting oceanic crust. Earth Planet. Science Lett. 143, 161–171.

Loucks, R.R., Mavrogenes, J.A., 1999. Gold solubility in supercritical hydrothermal brines measured in synthetic fluid inclusions. Science 284, 2159–2163.

Luth, W.C., Ingamells, O., 1965. Gel preparation of starting materials for hydrothermal experimentation. Am. Mineral. 50, 255–258.

Manning, C.E., 1994. The solubility of quartz in the lower crust and upper mantle. Geochim. Cosmochim. Acta 58, 4831–4839.

Manning, C.E., 1998. Fluid composition at the blueschist-eclogite transition in the model system Na_2O–MgO–Al_2O_3–SiO_2–H_2O–HCl. Swiss Bull. Mineral. Petrol. 78, 225–242.

Manning, C.E., 2004a. The chemistry of subduction-zone fluids. Earth Planet. Sci. Lett. 223, 1–16.

Manning, C.E., 2004b. Polymeric silicate complexing in aqueous fluids at high pressure and temperature, and its implications for water–rock interaction. In: Wanty, R.B., Seal II, R.R. (Eds.), Water–Rock Interaction. Proc. 11th Int. Symp. Water-rock Int., London, pp. 45–49.

Nichols, G.T., Wyllie, P.J., Stern, C.R., 1994. Subduction zone melting of pelagic sediments constrained by melting experiments. Nature 371, 785–788.

Nichols, G.T., Wyllie, P.J., Stern, C.R., 1996. Experimental melting of pelagic sediment, constraints relevant to subduction. In: Bebout, G.E., Scholl, D.H., Kirby, S.P., Platt, J. (Eds.), Subduction: Top to Bottom. . Geophys. Mon., vol. 96. American Geophysical Union, Washington, DC, pp. 293–298.

Ono, S., 1998. Stability limits of hydrous minerals in sediment and mid-ocean ridge basalt compositions; implications for water transport in subduction zones. J. Geophys. Res. 103, 18253–18267.

Pawley, A.R., 1992. Experimental study of the compositions and stabilities of synthetic nyböite and nyböite–glaucophane amphiboles. Eur. J. Mineral. 4, 171–192.

Pettke, T., Heinrich, C.A., Cioccan, A.C., Günther, D., 2000. Quadrupole mass spectrometry and optical emission spectrometry: detection capabilities and representative sampling of short transient signals from laser ablation. J. Anal. At. Spectrom. 15, 1149–1155.

Plank, T., Langmuir, C.H., 1993. Tracing trace elements from sediment input to volcanic output at subduction zones. Nature 362, 739–743.

Plank, T., Langmuir, C.H., 1998. The chemical composition of subducting sediment and its consequences for the crust and mantle. Chem. Geol. 145, 325–394.

Poli, S., Schmidt, M.W., 2002. Petrology of subducted slabs. Annu. Rev. Earth Planet. Sci. 30, 207–235.

Rea, D.K., Ruff, L.J., 1996. Composition and mass flux of sediment entering the world's subduction zones: implications for global sediment budgets, great earthquakes, and volcanism. Earth Planet. Sci. Lett. 140, 1–12.

Rubatto, D., Hermann, J., 2003. Zircon formation during fluid circulation in eclogites (Monviso, Western Alps): implications for Zr and Hf budget in subduction zones. Geochim. Cosmochim. Acta 67, 2173–2187.

Ryerson, F.J., Watson, E.B., 1987. Rutile saturation in magmas: implications for Ti–Nb–Ta depletion in island-arc basalts. Earth Planet. Sci. Lett. 86, 225–239.

Scambelluri, M., Philippot, P., 2001. Deep fluids in subduction zones. Lithos 55, 213–227.

Scambelluri, M., Fiebig, J., Malaspina, N., Müntener, O., Pettke, T., 2004. Serpentinite subduction: implications for fluid processes and trace element recycling. Int. Geol. Rev. 46, 595–613.

Schmidt, M.W., Vielzeuf, D., Auzanneau, E., 2004. Melting and dissolution of subducted crust at high pressures: the key role of white mica. Earth Planet. Sci. Lett. 228, 65–84.

Simon, A.C., Frank, M.R., Pettke, T., Candela, P.A., Piccoli, P.M., Heinrich, C.A., 2005. Gold partitioning in melt-vapor-brine systems. Geochim. Cosmochim. Acta 69, 3321–3335.

Spandler, C.J., Hermann, J., Arculus, R.J., Mavrogenes, J.A., 2003. Redistribution of trace elements during prograde metamorphism from lawsonite blueschist to eclogite facies; implications for deep subduction-zone processes. Contrib. Mineral. Petrol. 146, 205–222.

Spandler, C.J., Hermann, J., Arculus, R.J., Mavrogenes, J.A., 2004a. Reply to comments on "Redistribution of trace elements during prograde metamorphism from lawsonite blueschist to eclogite facies: implications for deep subduction zone processes". Contrib. Mineral. Petrol. 148, 506–509.

Spandler, C.J., Hermann, J., Arculus, R.J., Mavrogenes, J.A., 2004b. Geochemical heterogeneity and element mobility in deeply subducted oceanic crust; insights from high-pressure mafic rocks from New Caledonia. Chem. Geol. 206, 21–42.

Stern, C.R., Wyllie, P.J., 1973. Water-saturated and undersaturated melting relations of a granite to 35 kilobars. Earth Planet. Sci. Lett. 18, 163–167.

Stern, R.J., Kohut, E., Bloomer, S.H., Leybourne, M., Fouch, M., Vervoort, J., 2006. Subduction factory processes beneath the Guguan cross-chain, Mariana Arc; no role for sediments, are serpentinites important? Contrib. Mineral. Petrol. 151, 202–221.

Sterner, S.M., Bodnar, R.J., 1984. Synthetic fluid inclusions in natural quartz; 1, Compositional types synthesized and applications to experimental geochemistry. Geochim. Cosmochim. Acta 48, 2659–2668.

Tatsumi, Y., 2005. The subduction factory; how it operates in the evolving Earth. GSA Today 15–7, 4–10.

Taylor, S.R., McLennan, S.M., 1985. The Continental Crust: Its Composition and Evolution. Blackwell, Oxford, p. 312.

Ulmer, P., Trommsdorff, V., 1999. Phase relations of hydrous mantle subducting to 300 km. In: Fei, Y., Bertka, N., Mysen, B.O. (Eds.), Mantle Petrology: Field Observations and High Pressure Experimentation. Geochem. Soc. Spec. Pub., vol. 6, pp. 259–281.

Watson, E.B., Harrison, T.M., 1983. Zircon saturation revisited, temperature and composition effects in a variety of crustal magma types. Earth Planet. Sci. Lett. 64, 295–304.

Withers, A.C., Kohn, S.C., Brooker, R.A., Wood, B.J., 2000. A new method for determining the P–V–T properties of high-density H_2O using NMR: results at 1.4–4.0 GPa and 700–1100 °C. Geochim. Cosmochim. Acta 64, 1051–1057.

Zack, T., Kronz, A., Foley, S.F., Rivers, T., 2002. Trace element abundances in rutiles from eclogites and associated garnet mica schists. Chem. Geol. 184, 97–122.